Microbiome

RESEARCH

Open Access

Alternate day fasting alleviates neuroinflammation in diabetic mice by regulating δ-valerobetaine-carnitine-microglia axis via enrichment of *Akkermansia muciniphila*

Kaiyan Gong[1], Shuhui Zhang[1], Yangjie Pan[1], Qingpeng Cai[1], Mengjun Wu[1], Xiaoli Yin[1], Jiahui Ma[2], Hao Ji[2], Zhen Wang[3], Wenjun Wu[4] and Hong Zheng[1*]

Abstract

Background Alternate day fasting (ADF) as a healthy dietary pattern has been reported to improve brain functions and behaviors, but the effect of ADF on diabetes-related brain disorders and the potential mechanisms remain unclear. In this study, we investigated the impact of ADF on neuroinflammation and exploratory behavior in type 1 diabetic (T1D) mice and explored the specific molecular mechanisms from the perspective of the gut microbiota and host metabolism.

Results ADF can effectively relieve neuroinflammation and exploratory behavioral disorders in T1D mice. According to fecal microbiota transplant and bacterial supplementation, we demonstrated that ADF-driven enrichment of *Akkermansia muciniphila* (AKK) was necessary for boosting exploratory behavior in T1D mice. The gut microbiota-derived metabolite δ-valerobetaine (VB) reduced hepatic carnitine synthesis by inhibiting BBOX, and caused exploratory behavioral disorders in mice. In vitro and in vivo studies revealed that AKK bacteria had the ability to consume VB, and thereby increased systemic carnitine level. In addition, carnitine was found to deplete lipid droplet accumulation in microglia by enhancing fatty acid oxidation and lipolysis, reduce neuroinflammation and neuron injury, and then increase exploratory behavior in T1D mice.

Conclusions Our study sheds light on the gut-liver-brain metabolic axis mechanism on the protective role of ADF in T1D-associated neuroinflammation and exploratory behavioral disorders and AKK bacteria exert as a key mediator.

Keywords Diabetes, Behavior, Fasting, Gut-brain axis, Neuroinflammation

*Correspondence:
Hong Zheng
123zhenghong321@163.com
Full list of author information is available at the end of the article

Graphical Abstract

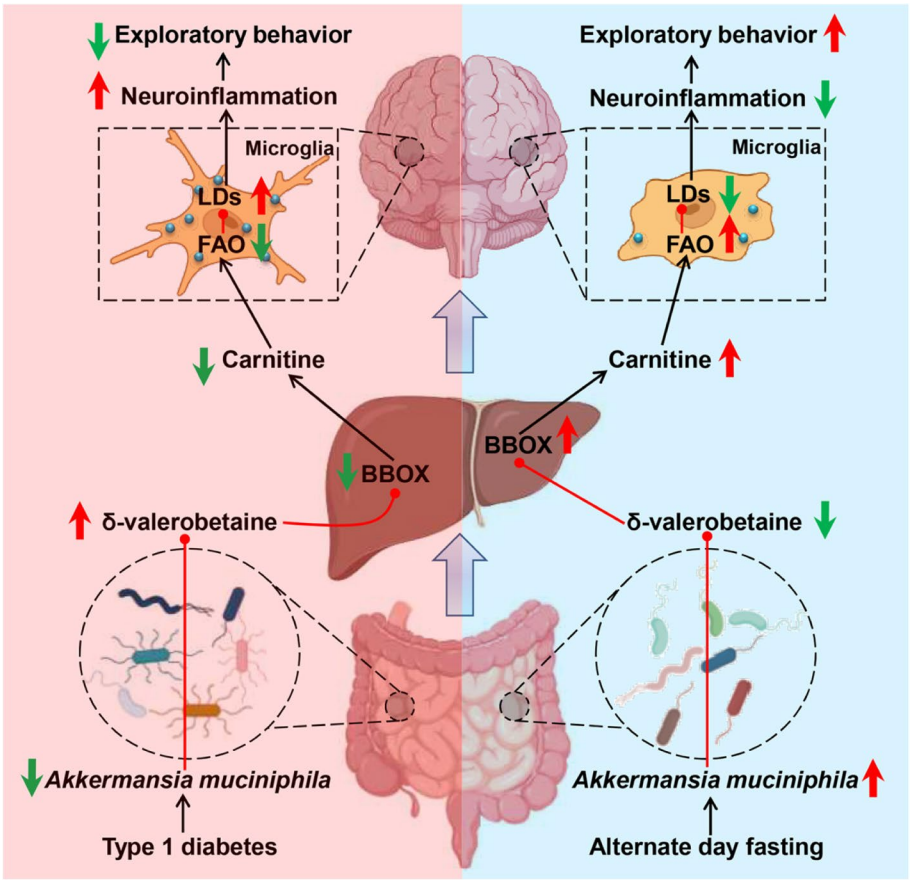

Introduction

Type 1 diabetes (T1D) is an autoimmune disease due to pancreatic β-cell destruction that leads to insulin deficiency and hyperglycemia [1]. The prevalence of T1D is globally increasing, and approximately 8.4 million individuals suffered from T1D in 2021 and this number will rise to 13.5–17.4 million in 2040 [1]. Of note, diabetes affects brain functions and behaviors, resulting in a higher risk of dementia [2, 3]. Some potential mechanisms on diabetic brain disorders have been proposed such as insulin resistance [4], oxidative stress [5], mitochondria damage [6], autophagy [7] and metabolic disturbances [8]. Besides, numerous studies have also reported that neuroinflammation plays a significant role in the onset and development of diabetic brain disorders [9, 10]. Compared to type 2 diabetes, however, neuroinflammation in T1D has received relatively less attention, posing a significant challenge to the care and management of brain health in T1D patients.

Accumulating evidence suggests that the gut microbiota and its metabolites modulate the gut-brain axis and exert as a key mediator for neuroinflammation [11]. Chen et al. reported that the gut microbiota imbalances promoted neuroinflammation via poly-unsaturated fatty acids and induced Alzheimer's disease (AD) pathologies in mice [12]. Xu et al. found that the gut dysbiosis contributed to depression-like behaviors by increasing neuroinflammation due to short-chain fatty acids (SCFAs) deficiency [13]. Aging-driven shifts in the gut bacteria caused microglia inflammation and behavior disorders through microbial metabolite TβMCA [14]. Previously, we also revealed that the gut microbiota from healthy mice reduced neuroinflammation and cognitive decline in T1D mice by increasing glutamate [15] and aspartate [16]. Besides, the impacts of the gut microbiota on neuroinflammation were also mediated by it metabolites SCFAs [17], indoles [18], glycerophospholipid [19] and obeticholic acid [20]. Thus it can be seen that the gut microbiota and its metabolites play a pivotal role in the

onset and progression of neuroinflammation, unveiling potential targets for the prevention and treatment of diabetes-induced behavioral disorders.

At present, scientists have proposed to mitigate neuroinflammation via targeted modulation of the gut microbiota. For example, dietary fiber as prebiotics has the ability to reshape the gut microbiota and increase SCFAs production and thereby attenuated neuroinflammation and cognitive impairment in mice [21]. Sun et al. reported that *Eucommiae* polysaccharides relieved diet-induced neuroinflammation and behavioral disorders of mice by regulating microbiota-driven tryptophan metabolism [22]. Polysaccharides from *Astragalus membranaceus* were found to alter microbial metabolites and alleviate LPS-induced neuroinflammation in mice [23]. In addition to prebiotics, probiotics also exhibited analogous effects, for example, supplementation with *Clostridium butyricum* decreased neuroinflammation in the AD mice via butyrate [24]. Kong et al. uncovered the ability of *Bifidobacterium longum* to enhance microbial kynurenine metabolism and then regulate neurotransmitters and neuroinflammation in autistic rats [25]. The antidepressant effect of *Bifidobacterium breve* was mediated through activating AhR by indole-3-lactate and decreasing neuroinflammation in mice [26]. More importantly, intermittent fasting (IF) is becoming a popular eating pattern that reshapes the gut microbiota and host metabolism and then exerts health-promoting effects on diabetes [27], cancer [28], hypertension [29], autoimmunity [30], and obesity [31]. In recent years, the protective role of IF in brain functions has also been revealed by targeting the gut microbial metabolism [32–34]. Therefore, IF-driven modulation of the gut microbiota might be a novel therapeutic avenue for nervous system diseases, thereby achieving the improvement of brain disorders through enteral therapy. Herein we hypothesized that alternate day fasting (ADF) may relieve neuroinflammation and boost exploratory behavior in T1D mice by regulating the gut-brain metabolic axis.

In this study, therefore, T1D mice were subjected to ADF, and the open field test was utilized to evaluate exploratory behavior. We found that ADF can effectively alleviate neuroinflammation and increase exploratory behavior in T1D mice. The protective effect of ADF might be mediate by enriching *Akkermansia muciniphila* and depleting microbial metabolite δ-valerobetaine (VB). Moreover, VB deficiency was found to increase systemic carnitine level and then decreased lipid droplets in microglia and inhibited neuroinflammation. Hence, our study not only proposed the potential of ADF for the prevention and management of neuroinflammation and exploratory behavioral disorders in T1D, but also disclosed a novel gut-liver-brain metabolic axis mechanism.

Results

ADF boosts exploratory behavior and alters the gut microbiota in T1D mice

In this study, we developed a mouse model of T1D induced by streptozotocin, and typical T1D symptoms were observed as indicated by significant increases in fasting blood glucose level (Figure S1a), daily food intake (Figure S1b) and daily water intake (Figure S1c), but a significant decrease in body weight (Figure S1d). To examine the effect of intermittent fasting (IF) on exploratory behavior, T1D and normal control (CON) mice were subjected to alternate day fasting (ADF) for 10 weeks, and the open field test (OFT) was used to assess exploratory behavior of mice, as shown in Fig. 1a. The OFT results reveal that T1D mice exhibited significantly lower exploratory behavior relative to CON mice, as indicated by reductions in the percentages of distance (Figs. 1b and 1c) and time (Figs. 1b and 1d) in center area and immobile time in edge area (Figs. 1b and 1e). However, after a 10-week ADF, these behavioral parameters in T1D mice were restored to normal levels, suggesting that ADF boosted exploratory behavior in T1D mice. ADF did not cause a significant impact on behavioral parameters in CON mice except immobile time in edge area (Figs. 1b-1f). There were no significant differences in immobile time in center area after ADF (Fig. 1f). In addition, ADF did not result in significant alterations in fasting blood glucose level (Figure S2a), daily food intake (Figure S2c) and daily water intake (Figure S2d) in CON mice, while their levels were significantly decreased in T1D mice after ADF. Body weight of CON mice was significantly lower after ADF, but there was no significant change in T1D mice (Figure S2b).

Subsequently, the changes in the gut microbiota were analyzed in T1D mice after ADF by using 16S rRNA gene sequencing. At the phylum level, the percentage of *Bacteroidetes* was decreased, but the percentages of *Firmicutes, Verrucomicrobia, Proteobacteria* and *Actinobacteria* were increased in both CON and T1D mice after ADF, as shown in Fig. 1g. These changes were more pronounced in T1D mice, for example, the percentage of *Verrucomicrobia* increased from 0.15% to 2.49% after ADF. At the genus level, the PCoA result shows a more distinct separation in the microbial pattern in T1D mice after ADF when compared with CON mice (Fig. 1h). Furthermore, we used the volcano plot to identify significantly altered microbes between CON and T1D mice (Figure S3a) as well as between T1D and T1D-IF mice (Figure S3b). The Venn diagram demonstrates that there were 15 gut microbes that significantly altered between CON and T1D mice but also varied in T1D mice after ADF (Figure S3c). Then, these 15 microbes were illustrated as a heatmap in Fig. 1i,

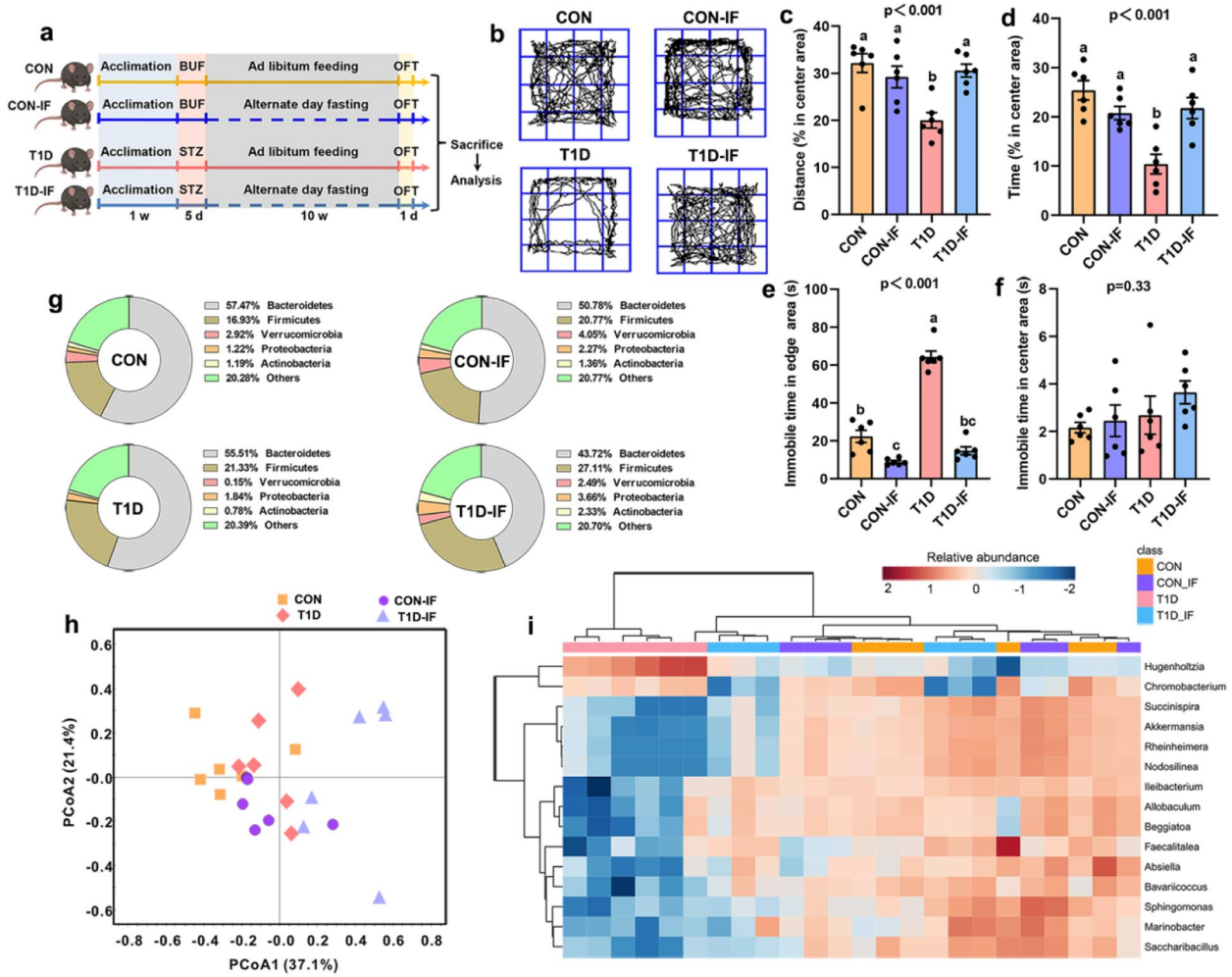

Fig. 1 Alternate day fasting boosts exploratory behavior and reshapes the gut microbiota in T1D mice. **a** Schematic diagram of the experimental procedure: After a one-week acclimation, T1D mice were developed by an intraperitoneal injection of streptozotocin (STZ) solution for 5 days, and the corresponding normal control (CON) mice were treated with the same volume of citrate buffer. Subsequently, T1D and CON mice were subjected to alternate day fasting (ADF) for 10 weeks and labeled as T1D-IF and CON-IF, respectively. After ADF, exploratory behavior was evaluated by the open field test (OFT) and then samples were collected for further analysis. **b**-**f** Changes in (**b**) the motion trails, the percentages of (**c**) distance and (**d**) time in center area as well as immobile time in (**e**) edge area and (**f**) center area in CON and T1D mice after ADF in the OFT ($n = 6$ per group). **g** The percentages of the gut microbiota at the phylum level in CON, CON-IF, T1D and T1D-IF mice ($n = 6$ per group). **h** Classification of the microbial patterns among different groups at the genus level by PCoA ($n = 6$ per group). **i** Heatmap showing gut microbes that significantly altered between CON and T1D mice and also varied in T1D mice after ADF ($n = 6$ per group). The significant of difference among CON, CON-IF, T1D and T1D-IF groups was analyzed using one-way ANOVA with a post-hoc Dunnett's test for multiple comparisons, and different lowercase letters represent a statistically significant difference between different groups ($p < 0.05$)

where we found that the relative abundances of most microbes markedly increased in T1D mice after ADF and remained at similar levels with CON and CON-IF mice, including *Succinispira, Akkermansia, Pheinheimera, Nodosilinea, IIeibacterium, Allobaculum, Beggiatoa, Faecalitalea, Absiella, Bavariicoccus, Sphigomonas, Marinobacter,* and *Saccharibacillus*. Therefore, our results imply that ADF has potential to reshape the gut microbiota and increase exploratory behavior in T1D mice.

ADF reduces neuroinflammation and neuron injury in the prefrontal cortex of T1D mice

Since the prefrontal cortex (PFC) is a primary brain region that contributes to exploratory behavior [35], we analyzed the effect of ADF on microglial activation and neuron injury in this region of T1D mice. The results show that the number of Iba-1 positive staining was significantly higher in the PFC of T1D mice relative to CON mice but markedly reduced after ADF (Figs. 2a and 2b), indicating that ADF suppressed T1D-induced microglial

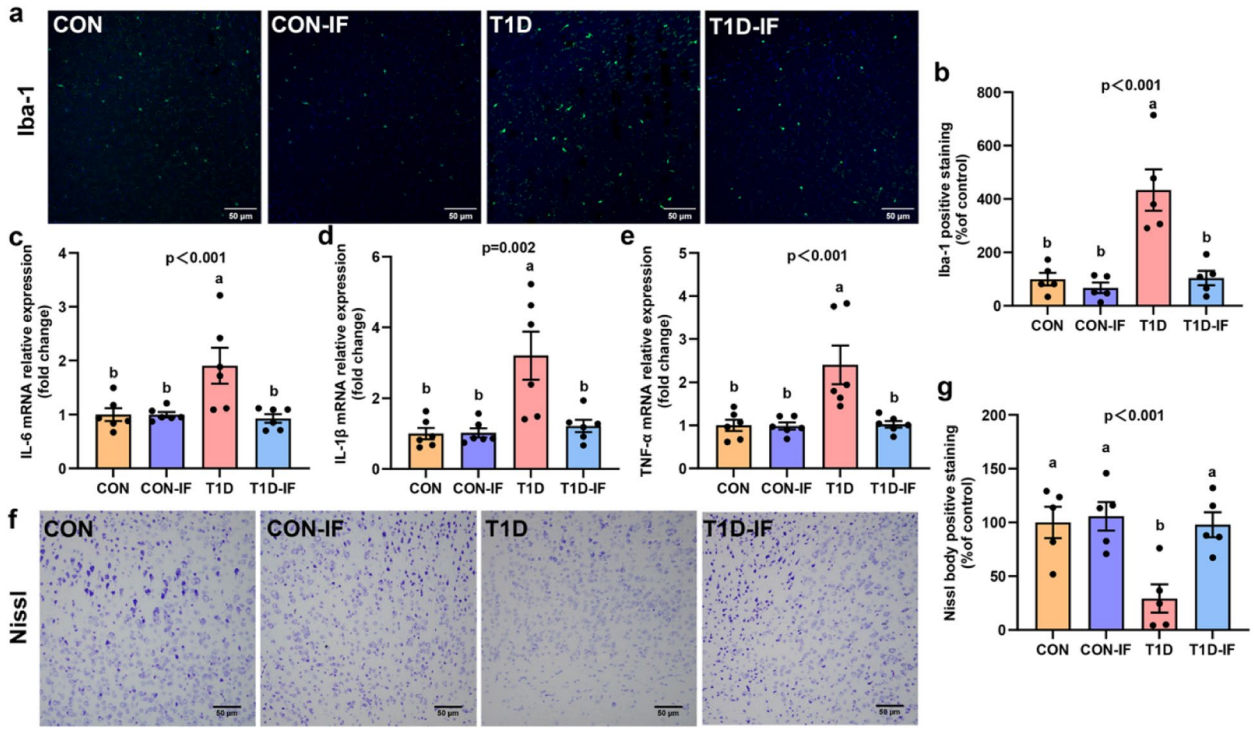

Fig. 2 Alternate day fasting mitigates neuroinflammation and neuron injury in the prefrontal cortex of T1D mice. **a**, **b** Representative images of Iba-1 immunofluorescence staining and the quantitative data in the prefrontal cortex (PFC) of normal control (CON) and type 1 diabetic (T1D) mice as well as alternate day fasting (ADF)-treated CON and T1D mice (CON-IF and T1D-IF) ($n = 5$ per group). **c**-**e** The mRNA expression levels of (**c**) IL-6, **d** IL-1β and (**e**) TNF-α in the PFC of CON, T1D, CON-IF and T1D-IF mice ($n = 6$ per group). **f**, **g** Representative images of Nissl body staining and the quantitative data in the PFC of CON, T1D, CON-IF and T1D-IF mice ($n = 5$ per group). The significant of difference among CON, CON-IF, T1D and T1D-IF groups was analyzed by one-way ANOVA with a post-hoc Dunnett's test for multiple comparisons, and different lowercase letters represent a statistically significant difference between different groups ($p < 0.05$)

activation in the PFC. This finding was further confirmed by the changes in proinflammatory factors, where we found that the mRNA expression levels of IL-6 (Fig. 2c), IL-1β (Fig. 2d) and TNF-α (Fig. 2e) were significantly higher in the PFC of T1D mice compared with CON mice but reduced to normal levels after ADF. Relative to CON mice, of note, the number of Nissl body positive staining was dramatically reduced in the PFC of T1D mice, which can be mitigated after ADF (Figs. 2f and 2g), implying that ADF protected against PFC neuron injury caused by T1D.

ADF reshapes host metabolism especially increased carnitine synthesis and fatty acid oxidation

Furthermore, we examined the metabolic changes in the PFC and serum of T1D mice following ADF by using an untargeted LC–MS-based metabolomics method. The PCA results reveal that ADF resulted in clear separations in the metabolic patterns of the PFC and serum between CON and T1D mice under both positive (Figs. 3a and 3b) and negative (Figures S4a and S4b) modes. Yet, interestingly, the PFC metabolic patterns in T1D mice after ADF were close to those in CON mice (Figs. 3a and S3a), suggesting that ADF reshaped T1D-induced PFC metabolic disorders. Then, using an integrated method of multivariate and univariate analyses, metabolites with VIP > 1.0, $P < 0.01$ and FC > 2.0 were selected as important metabolites as illustrated in Figure S5a for PFC and Figure S5b for serum. After ADF, the levels of most metabolites in the PFC and serum did not obviously alter in CON mice, but were significantly reversed in T1D mice (Figures S5a and S5b). The metabolite set enrichment analysis was performed to achieve the functional classification of these metabolites, and top 10 enriched metabolic functions in the PFC and serum were presented in Figs. 3c and 3d, respectively. We identified 3 common enriched metabolic functions in the PFC and serum, including oxidation of branched chain fatty acids, beta oxidation of very long chain fatty acids, and carnitine synthesis. In these metabolic functions, carnitine is a common metabolite involved in regulating fatty acid oxidation (FAO, Fig. 3e).

Afterward, we developed a targeted analytical method of carnitine, and the retention time and MS/MS fragment

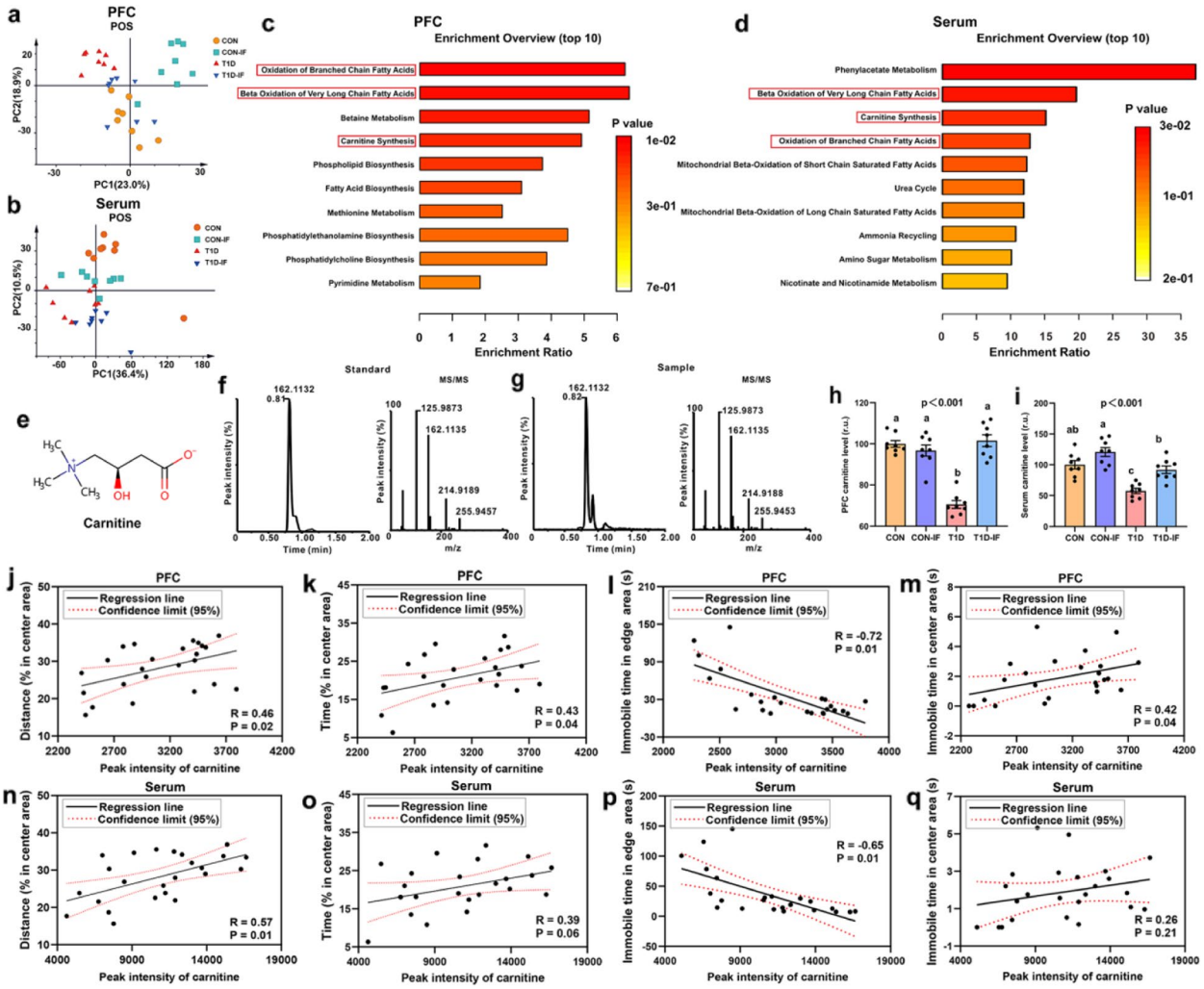

Fig. 3 Alternate day fasting reshapes host metabolism in T1D mice. **a**, **b** PCA classification of the metabolic patterns of the (**a**) prefrontal cortex (PFC) and (**b**) serum detected using LC–MS-based untargeted metabolomics under positive mode in normal control (CON) and type 1 diabetic (T1D) mice as well as alternate day fasting (ADF)-treated CON and T1D mice (CON-IF and T1D-IF) ($n = 8$ per group). **c**, **d** Top 10 important metabolic functions in the (**c**) PFC and (**d**) serum analyzed by the metabolite set enrichment analysis based on key metabolites. **e** Molecular structure of carnitine. **f**, **g** The retention time and MS/MS fragment ions of (**f**) carnitine standard substance and (**g**) carnitine in biological samples using LC–MS analysis. **h**, **i** Changes in the carnitine level in the (**h**) PFC and (**i**) serum of CON, CON-IF, T1D and T1D-IF mice ($n = 8$ per group). **j**-**q** Correlations between the percentages of (**j**, **n**) distance and (**k**, **o**) time in center area as well as immobile time in (**l**, **p**) edge area and (**m**, **q**) center area in the OFT and carnitine in the PFC and serum of mice. The significant of difference among CON, CON-IF, T1D and T1D-IF groups was analyzed by one-way ANOVA with a post-hoc Dunnett's test for multiple comparisons, and different lowercase letters represent a statistically significant difference between different groups ($p < 0.05$)

ions of carnitine in biological samples closely matched those of the standard substance, indicating high reliability and specificity of the analytical method (Figs. 3f and 3g). The results of quantitative analysis demonstrate that T1D mice had significantly lower levels of carnitine in the PFC (Fig. 3h) and serum (Fig. 3i) than CON mice, which can be reversed to normal levels after ADF. Yet, ADF did not significantly alter the carnitine levels in the PFC and serum in CON mice. Additionally, we found that the level of carnitine in the PFC was significantly and positively correlated with the percentages of distance (Fig. 3j) and time (Fig. 3k) in center area and immobile time in center area (Fig. 3m), but negatively linked with immobile time in edge area (Fig. 3l). The significant positive associations were also detected between the serum carnitine level and the percentages of distance (Fig. 3n) and time (Fig. 3o) in center area. The level of carnitine in the serum was negatively related to immobile time in edge area (Fig. 3p), while no significant correlation was observed with immobile time in center area (Fig. 3q).

These results indicate that increased carnitine level may contribute to the improvement of exploratory behavior in T1D mice. Taken together, our findings suggest that ADF may increase systemic carnitine level and FAO, and thereby reduce neuroinflammation and boost exploratory behavior in T1D mice.

Microbial metabolite δ-valerobetaine suppresses hepatic carnitine synthesis and reduces exploratory behavior

Carnitine is mainly synthesized via the hydroxylation of γ-butyrobetaine (γBB) by γBB hydroxylase (BBOX) in the liver (Fig. 4a). After ADF, we found a significant increase in the mRNA expression level of BBOX in the liver of T1D mice (Fig. 4b), which could be responsible to ADF-driven increase in the carnitine level. To examine the relationship of carnitine with other metabolites, Spearman correlation analysis was carried out, and the results reveal that carnitine had a significant negative correlation with δ-valerobetaine (VB), a gut microbial metabolite [36], as shown in Fig. 4c. According to molecular docking analysis, the estimated binding free energy of VB (−6.61 kcal/mol) was found to be higher than that of γBB (−5.67 kcal/mol) (Fig. 4d). This result indicates that VB may competitively inhibit the binding site of γBB to BBOX, which is in agreement with the finding of Zhao et al. [37]. In addition, we observed a significant positive correlation between carnitine and the neurotransmitter glutamine (Fig. 4c). However, whether the beneficial effects of carnitine were mediated by promoting glutamine production remains to be further explored.

To investigate the effect of VB on carnitine synthesis and exploratory behavior, CON mice were subjected to an intraperitoneal injection of VB for 3 weeks (Fig. 4e). The results show that the level of carnitine was significantly reduced in the serum (Fig. 4f) and PFC (Fig. 4g) after VB treatment. The immunohistochemical analysis reveals that the number of BBOX positive staining was notably decreased in the liver of mice following VB treatment (Figs. 4h and 4i), implying that VB may reduce hepatic BBOX protein level. According to the OFT experiments, we found that VB reduced exploratory behavior in mice, as indicated by significantly lower percentages of distance (Figs. 4j and 4k) and time (Figs. 4j and 4l) in center area as well as immobile time in center area (Fig. 4n). Moreover, treatment with VB resulted in an increase in immobile time in edge area in mice (Fig. 4m). To analyze the impact of VB on carnitine synthesis in vitro, AML12 hepatocytes were treated with VB for 24 h (Figure S6a). After VB treatment, the levels of carnitine (Figure S6b) and BBOX mRNA expression (Figure S6c) were significantly decreased in AML12 cells. Therefore, we speculated that microbial metabolite VB can suppress hepatic carnitine synthesis, thereby lowering systemic carnitine level and exploratory behavior of mice.

ADF-driven enrichment of *Akkermansia muciniphila* increases exploratory behavior by consuming δ-valerobetaine

To inspect the causal role of the gut microbiota in the protective effect of ADF on exploratory behavior, T1D mice were transplanted with fecal microbiota from either T1D mice (T1D-R) or ADF-treated T1D mice (ADF-R) for 10 weeks (Fig. 5a). Relative to T1D-R mice, the percentage of *Firmicutes* was reduced in ADF-R mice, while increases in the percentages of *Bacteroidetes, Proteobacteria, Verrucomicrobia* and *Actinobacteria* were obtained (Figure S7). A clear separation in the microbial pattern was detected between T1D-R and ADF-R mice by using PCoA (Fig. 5b). At the genus level, we focused on analyzing the gut microbes that significantly reversed in T1D mice after ADF as presented in Fig. 1i, where 6 gut microbes were still identified after fecal microbiota transplant (FMT), including *Akkermansia, lleibacterium, Sphingomonas, Nodosilinea_PCC-7104, Allobaculum,* and *Faecalitalea* (Fig. 5c). Among them, *Akkermansia* exhibited the highest relative abundance and its level was significantly increased in ADF-R mice compared with T1D-R mice, indicating successful colonization of *Akkermansia* into T1D mice after FMT (Fig. 5c). Besides, ADF-R mice had a lower level of fecal VB (Figure S8a) and higher levels of PFC carnitine (Figure S8b), serum carnitine (Figure S8c) and BBOX mRNA expression (Figure S8d) than T1D-R mice. Relative to T1D-R mice, the number of Iba-1 positive staining was markedly reduced in the PFC of ADF-R mice (Figures S8e and S8f). The PFC levels of IL-6 (Figure S8g), IL-1β ($p=0.26$, Figure S8h) and TNF-α (Figure S8i) were also observed to be decreased in ADF-R mice. Since 4-hydroxynonenal (4-HNE) is an end-product of lipid peroxidation, the level of 4-HNE positive staining in the PFC was significantly decreased in ADF-R mice when compared with T1D-R mice (Figures S8j and S8k), suggesting that FMT from ADF-treated mice can alleviate lipid peroxidation in the PFC of T1D mice. The Nissl staining results show that T1D-R mice had a significantly lower level of Nissl body positive staining in the PFC than ADF-R mice (Figures S8j and S8l). We also found that FMT from ADF-treated mice increased exploratory behavior in T1D mice, as indicated by significantly higher percentages of distance (Figs. 5d and 5e) and time (Figs. 5d and 5f) in center area and immobile time in center area (Fig. 5h), but significantly decreased immobile time in edge area (Fig. 5g).

To verify the effect of *Akkermansia* on carnitine synthesis and exploratory behavior, T1D mice were

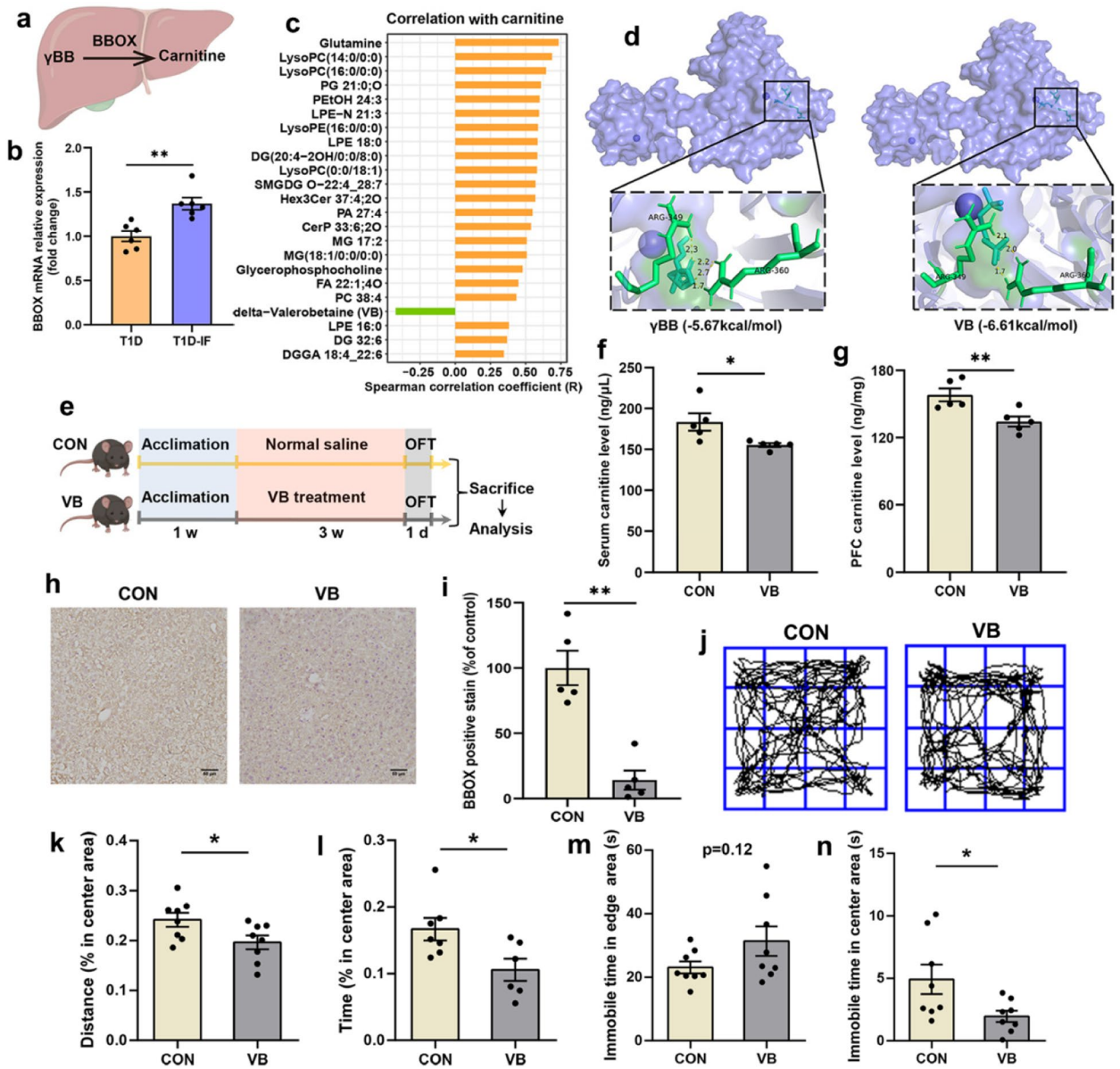

Fig. 4 Treatment with δ-valerobetaine inhibits hepatic carnitine synthesis and reduces exploratory behavior in mice. **a** Carnitine is mainly synthesized via the hydroxylation of γ-butyrobetaine (γBB) by γBB hydroxylase (BBOX) in the liver. **b** The mRNA expression level of BBOX in the liver of type 1 diabetic (T1D) mice and alternate day fasting (ADF)-treated T1D mice ($n = 6$ per group). **c** Spearman correlation coefficient of carnitine with other key metabolites ($p < 0.05$). **d** The estimated binding free energy of γBB and δ-valerobetaine (VB) analyzed by molecular docking analysis. **e** Schematic diagram of the experimental procedure: After a one-week acclimation, normal control (CON) mice were subjected to an intraperitoneal injection of either VB or saline vehicle for 3 weeks. Subsequently, exploratory behavior was evaluated by the open field test (OFT) and samples were collected for further analysis. **f**, **g** The carnitine levels in the (**f**) serum and (**g**) prefrontal cortex (PFC) of CON and VB-treated mice ($n = 5$ per group). **h**, **i** Representative images of BBOX immunohistochemistry staining and the quantitative data in the liver of CON and VB-treated mice ($n = 5$ per group). **j**-**n** Changes in (**j**) the motion trails and the percentages of (**k**) distance and (**l**) time in center area as well as immobile time in (**m**) edge area and (**n**) center area in CON and VB-treated mice in the OFT ($n = 8$ per group). The significant of difference between two groups was analyzed by two-tailed unpaired student's *t* test. Significant level: $^{*}p < 0.05$, $^{**}p < 0.01$

administered *Akkermansia muciniphila* (AKK) via oral gavage for 8 weeks (Fig. 5i). After an 8-week AKK treatment, the relative abundance of AKK bacteria was dramatically increased (Fig. 5j), suggesting successful colonization of AKK bacteria. In addition, we found that the levels of VB in the feces (Fig. 5k), serum (Fig. 5l) and liver (Fig. 5m) were significantly reduced in T1D mice, while the levels of carnitine in the liver (Fig. 5n)

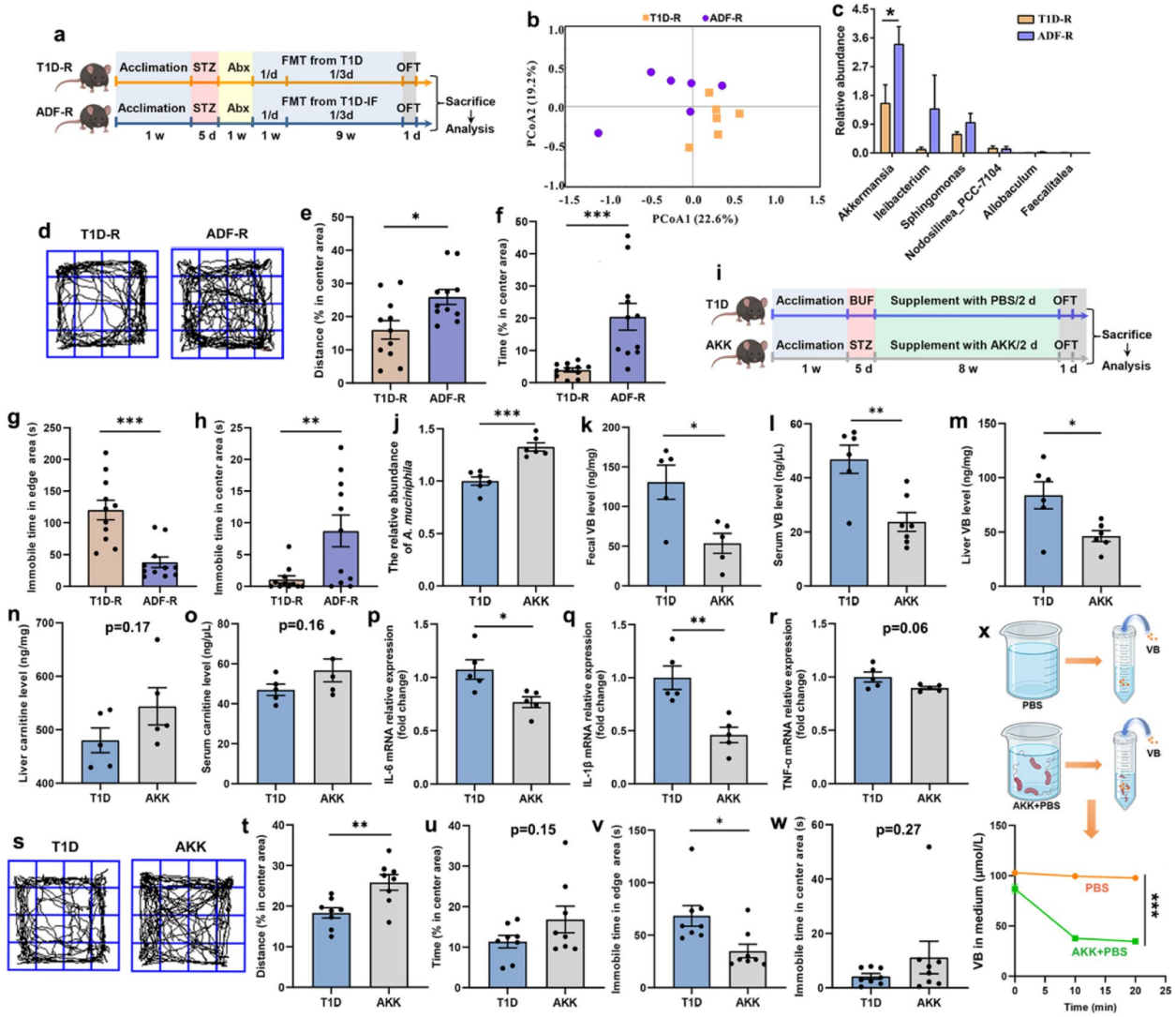

Fig. 5 Alternate day fasting-driven enrichment of *Akkermansia muciniphila* improves exploratory behavioral disorders in T1D mice. **a** Schematic diagram of the experimental procedure: The recipient T1D mice were given an antibiotic cocktail (Abx) to deplete their endogenous gut bacteria for one week, and then transplanted with fecal microbiota from T1D mice (T1D-R) or alternate day fasting (ADF)-treated T1D mice (ADF-R) once a day for the first week and every three days for 9 weeks. The open field test (OFT) was performed to evaluate exploratory behavior of mice and samples were collected for further analysis. **b** Classification of the microbial patterns between T1D-R and ADF-R mice at the genus level by PCoA ($n = 6$ per group). **c** The relative abundances of gut microbes that significantly reversed in T1D mice after ADF and still identified after fecal microbiota transplant ($n = 6$ per group). (d-h) Changes in (**d**) the motion trails and the percentages of (**e**) distance and (**f**) time in center area as well as immobile time in (**g**) edge area and (**h**) center area in T1D-R and ADF-R mice in the OFT ($n = 11$ per group). **i** Schematic diagram of the experimental procedure: T1D mice were orally administered with either sterile PBS or bacterial suspension of *A. muciniphila* (AKK) every other day for 8 weeks, and then exploratory behavior was evaluated by the OFT and samples were collected for further analysis. **j** Changes in the relative abundance of *A. muciniphila* in T1D mice after a 8-week AKK supplementation ($n = 6$ per group); **k**-**m** The level of δ-valerobetaine (VB) in the (**k**) feces ($n = 5$ per group), **l** serum ($n = 6$ per group) and (**m**) liver ($n = 6$ per group) of T1D mice and AKK-treated T1D mice. **n**, **o** The level of carnitine in the (**n**) liver and (**o**) serum of T1D mice and AKK-treated T1D mice ($n = 5$ per group). **p**-**r** The mRNA expression levels of (**p**) IL-6, **q** IL-1β and (**r**) TNF-α in the prefrontal cortex of T1D mice and AKK-treated T1D mice ($n = 5$ per group). **s**-**w** Changes in (**s**) the motion trails and the percentages of (**t**) distance and (**u**) time in center area as well as immobile time in (**v**) edge area and (**w**) center area in T1D mice and AKK-treated T1D mice in the OFT ($n = 8$ per group). **x** Changes in the concentration of VB in AKK bacterial suspension and PBS solution after 10 and 20 min ($n = 4$ per group). The significant of difference between two groups was analyzed by two-tailed unpaired student's *t* test. The significant of difference in the changes of the VB concentration with time was evaluated by a repeated measure ANOVA. Significant level: $^{*}p < 0.05$, $^{**}p < 0.01$, $^{***}p < 0.001$

and serum (Fig. 5o) were increased. These findings suggest that AKK bacteria may potentially consume VB and thereby increase carnitine synthesis. Moreover, the levels of IL-6 (Fig. 5p), IL-1β (Fig. 5q) and TNF-α (Fig. 5r) were reduced in the PFC of T1D mice after AKK treatment. In the OFT experiments, we observed increases in the percentages of distance (Figs. 5s and 5t) and time (Figs. 5s and 5u) in center area and immobile time in center area (Fig. 5w) as well as a decrease in immobile time in edge area (Fig. 5v), indicating that AKK bacteria may boost exploratory behavior in T1D mice. To further confirm whether AKK bacteria can consume VB, we added VB into AKK bacterial suspension or PBS solution, and measured the concentration of VB in the solution after 10 and 20 min (Fig. 5x). The results demonstrate that the VB level was significantly reduced in AKK bacterial suspension relative to PBS solution (Fig. 5x), implying that AKK bacteria have the ability to deplete VB. Consequently, we speculated that AKK bacteria enriched by ADF relieved neuroinflammation and enhanced exploratory behavior in T1D mice by regulating the VB-carnitine metabolic axis.

Carnitine inhibits neuroinflammation via reducing lipid droplets in microglia and increases exploratory behavior

To explore the protective mechanism of carnitine (CAR) on exploratory behavior, T1D mice were treated with intraperitoneal injection of CAR for 10 weeks (Fig. 6a). Considering the fact that CAR is a key mediator in long-chain FAO [38], we analyzed the change of lipid droplets in microglia of the PFC in T1D mice after CAR treatment via immunofluorescent staining. The results illustrates that the percentage of cells co-localizing Iba-1 and BODIPY was dramatically lower in the PFC of T1D mice treated with CAR (Figs. 6b and 6c). Moreover, a significant reduction in the number of Iba-1 positive staining was also observed in CAR-treated T1D mice (Figs. 6b and 6d). Neuroinflammation in the PFC of T1D mice was ameliorated after CAR treatment, as indicated by significantly lower levels of IL-6 (Fig. 6e), IL-1β (Fig. 6f) and TNF-α (Fig. 6g) in CAR-treated T1D mice. It can be seen from the immumohistochemical results that T1D mice exhibited a significantly decrease in the number of 4-HNE positive staining (Figs. 6h and 6j) and increase in Nissl body positive staining (Figs. 6i and 6k) in the PFC after CAR treatment, indicating that CAR relieved T1D-induced lipid peroxidation and neuron injury in the brain. Additionally, the percentages of distance (Figs. 6l and 6m) and time (Figs. 6l and 6n) in center area and immobile time in center area ($p=0.18$, Fig. 6p) were increased but immobile time in edge area (Fig. 6o) was decreased in CAR-treated T1D mice, manifesting the improvement of exploratory behavior. Furthermore, we analyzed the effect of CAR on PFC lipid metabolism in T1D mice, and found that CAR treatment can considerably increase the expression levels of genes related to fatty acid β-oxidation (Fig. 6q; e.g. CPT1b, ACACA) and lipolysis (Fig. 6r; e.g. ATGL, HSL, PLIN3). Nevertheless, fatty acid synthesis (e.g. ACC1, DGAT) was not significantly altered in the PFC of T1D mice after CAR treatment (Fig. 6s).

Furthermore, in vitro studies were utilized to further verify the effect of CAR on lipid droplets and inflammatory response in microglial cells. High glucose (HGlu) stimulation significantly increased BV2 cell viability at the concentrations of 35, 45 and 55 mM (Figures S9a and S9b), while CAR treatment can attenuate HGlu-induced increase in BV2 cell viability especially at a concentration of 10 μM (Figures S9c and S9d). Hence, 35 mM glucose and 10 μM CAR were selected for subsequent BV2 cell experiments. Next, BV2 cells were pretreated with CAR for 2 h and then cultured under HGlu condition for 12 h, as illustrated in Figure S10a. The immunofluorescent staining shows that the percentage of BV2 cells co-localizing Iba-1 and BODIPY was notably reduced after CAR treatment, suggesting that CAR can reduce lipid droplet accumulation in HGlu-treated BV2 cells (Figures S10b and S10c). Under HGlu condition, BV2 cells treated with CAR had significant decreases in intracellular and extracellular levels of pro-inflammatory cytokines, including IL-6 (Figures S11a and S11d), IL-1β (Figure S11b) and TNF-α (Figures S11c and S11e). Consistent with in vivo results, CAR notably increased the expression levels of genes related to fatty acid β-oxidation (Figure S12a; e.g. CPT1b, ACACA) and lipolysis (Figure S12b; e.g. ATGL, HSL) in HGlu-treated BV2 cells. Besides, the reductions in mRNA expression levels of ACC1 and DGAT (Figure S12c) indicated a lower fatty acid synthesis in CAR-treated BV2 cells under HGlu condition. To investigate whether VB directly induces neuroinflammation, BV2 cells were treated with VB and the expression levels of pro-inflammatory factors were analyzed after 12 h (Figure S13a). After VB treatment, the mRNA expression levels of IL-6 (Figure S13b), IL-1β (Figure S13c) and TNF-α (Figure S13d) were not significantly altered in BV2 cells, suggesting that VB may not directly lead to neuroinflammation. Collectively, we elucidated that CAR improved neuroinflammation and exploratory behavior in T1D mice by reducing lipid droplets in microglia.

Discussion

Intermittent fasting (IF) has been recognized as a healthy dietary pattern that can improve brain functions and behaviors [32]. In this study, we reported that ADF as a type of IF relieved neuroinflammation and boosted exploratory behavior in T1D mice by normalizing the

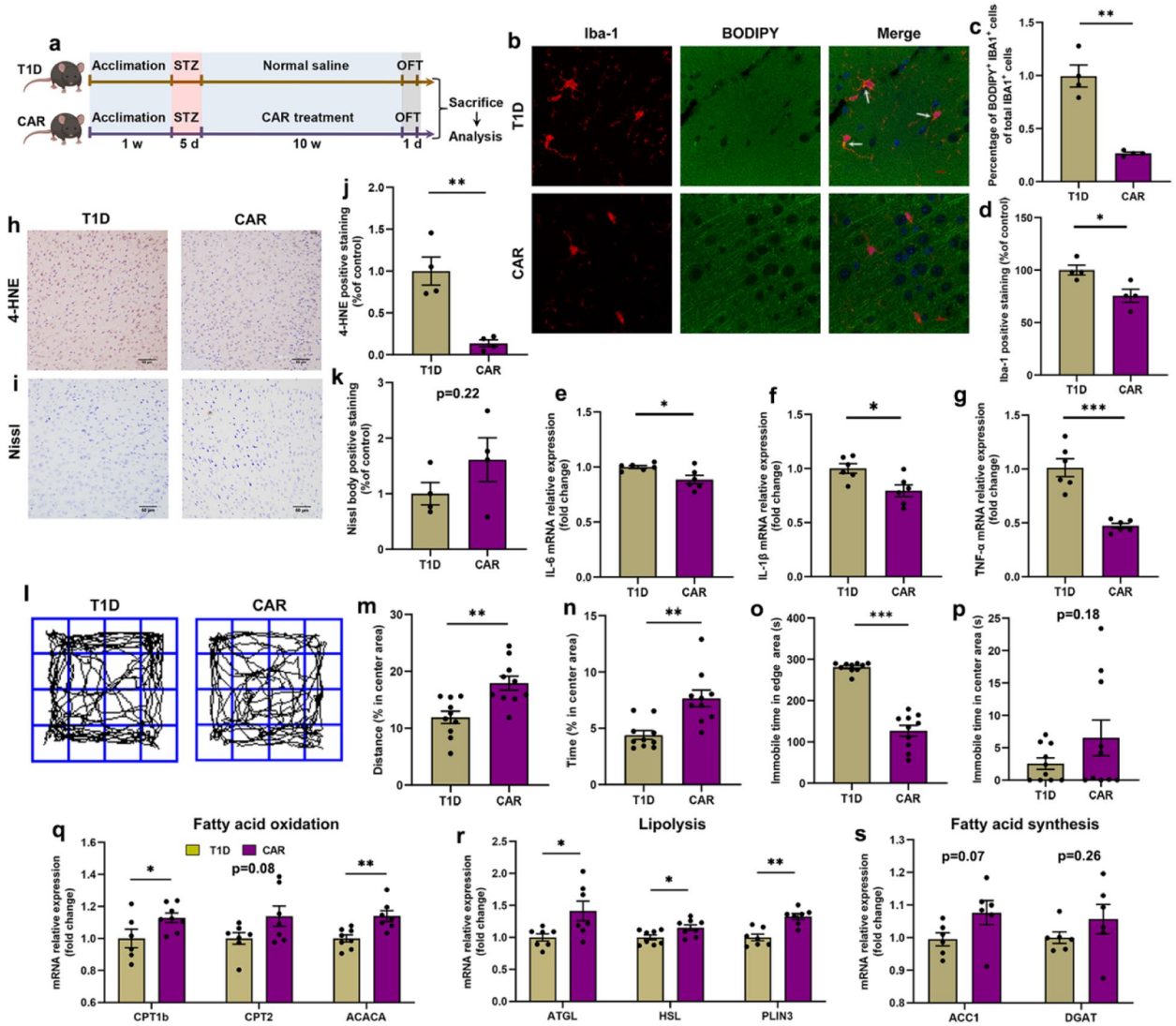

Fig. 6 Treatment with carnitine reduces neuroinflammation and exploratory behavioral disorders in T1D mice. **a** Schematic diagram of the experimental procedure: T1D mice were subjected to an intraperitoneal injection of either carnitine (CAR) or saline vehicle for 10 weeks. Then, exploratory behavior was evaluated by the open field test (OFT) and samples were collected for further analysis. **b**-**d** Representative images of Iba-1 and BODIPY staining and the corresponding quantitative data in the prefrontal cortex (PFC) of T1D and CAR-treated T1D mice ($n = 4$ per group). **e**–**g** The mRNA expression levels of (**e**) IL-6, **f** IL-1β and (**g**) TNF-α in the PFC of T1D and CAR-treated T1D mice ($n = 6$ per group). **h**–**k** Representative images of (**h**, **j**) 4-HNE and (**i**, **k**) Nissl body staining and the corresponding quantitative data in the prefrontal cortex (PFC) of T1D and CAR-treated T1D mice ($n = 4$ per group). **l**-**p** Changes in (**l**) the motion trails and the percentages of (**m**) distance and (**n**) time in center area as well as immobile time in (**o**) edge area and (**p**) center area in T1D and CAR-treated T1D mice in the OFT ($n = 10$ per group). **q**-**s** The mRNA expression levels of genes related to (**q**) fatty acid β-oxidation (CPT1b, CPT2 and ACACA), (r) lipolysis (ATGL, HSL and PLIN3), and (**s**) fatty acid synthesis (ACC1 and DGAT) ($n = 6$–8 per group). The significant of difference between two groups was analyzed by two-tailed unpaired student's *t* test. Significant level: $^{*}p < 0.05$, $^{**}p < 0.01$, $^{***}p < 0.001$

gut-liver-brain metabolic axis (Fig. 7). ADF increased systemic carnitine level and reduced microglial activation in the PFC of T1D mice. Hepatic carnitine synthesis was mediated by the gut microbiota-derived metabolite VB via inhibiting BBOX, and treatment with VB decreased exploratory behavior in mice. Using fecal microbiota transplant and AKK supplementation, we proved that ADF-driven enrichment of AKK bacteria was necessary for improving exploratory behavior in T1D mice. We also revealed that AKK bacteria may consume VB by in vitro and in vivo studies and thereby increased systemic carnitine level. Moreover, the carnitine treatment was found to decrease lipid droplet accumulation in microglia by enhancing fatty acid oxidation (FAO) and lipolysis,

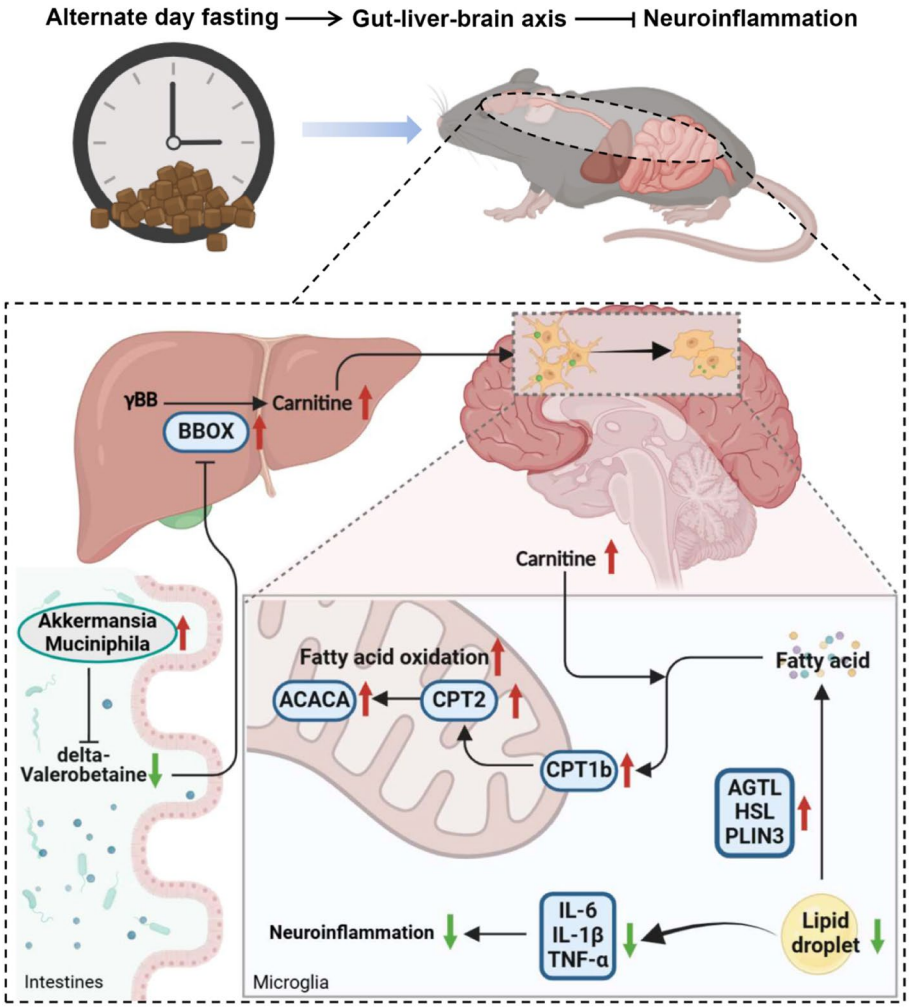

Fig. 7 Schematic diagram on the protective effect of alternate day fasting on exploratory behavioral disorders in T1D mice via the gut-liver-brain axis. Alternate day fasting (ADF) can increase systemic carnitine level through the enrichment of *Akkermansia muciniphila* (AKK), which has the potential to consume microbial metabolite δ-valerobetaine (VB). Subsequently, carnitine reduces lipid droplet accumulation in microglia by enhancing fatty acid oxidation and lipolysis, lowers neuroinflammation, and then increases exploratory behavior

relieve neuroinflammation and neuron injury, and then increased exploratory behavior in T1D mice. Consequently, our results shed light on the protective effect of ADF on neuroinflammation and exploratory behavioral disorders in T1D via the crosstalk of microbial metabolite VB, carnitine and microglia.

In recent years, numerous studies illuminated that the gut microbiota can mediate the beneficial effects of IF on brain functions through regulating host metabolism. Liu et al. reported that ADF reduced cognitive decline in T2D mice by remodeling the gut microbiota and its metabolites, including 3-indolepropionic acid, serotonin, and SCFAs [39]. IF has been also shown to enrich probiotics *Lactobacillus*, decrease carbohydrate metabolism and increase amino acid metabolism, thereby alleviating AD-like pathology and cognitive decline in an AD mouse model [33]. Here we found that ADF markedly facilitated hepatic carnitine production and increased systemic carnitine level in T1D mice. Later, carnitine enhanced FAO and lipolysis and then reduced lipid droplets in microglia. It has been reported that carnitine plays a vital role in long-chain FAO [38] and the accumulation of lipid droplets in microglia has been proved as a key trigger for neuroinflammation [40]. In addition, the therapeutic effects of carnitine on neurological and psychiatric diseases have been widely proved by improving oxidative stress, inflammatory response, mitochondrial dysfunction, neurotransmission and fatty acid transport [41]. Herein our results suggest that ADF lowered neuroinflammation by promoting carnitine-mediated FAO and depleting

lipid droplets in microglia, and then boosted exploratory behavior in T1D mice. In this process, metabolite VB was identified to exert a crucial mediating effect. Of note, VB has been confirmed to originate from the gut microbiota and inhibit hepatic carnitine synthesis and FAO [36]. Microbial metabolite VB exerts a crucial role in human health and disease [42]. For example, VB inhibited hepatic BBOX expression, decreased carnitine synthesis and FAO, and resulted in liver steatosis [37] and cardiac hypertrophy [43]. Additionally, VB has also been revealed to impair glucose metabolism [44], energy metabolism [45] and neuronal function [46]. In this study, we demonstrated another detrimental effect of VB that reduces exploratory behavior in T1D mice by lowering hepatic carnitine synthesis, suppressing carnitine-driven FAO in microglia and inducing neuroinflammation.

Another interesting finding in this study reveals that AKK bacteria can be enriched after ADF, which is essential for protection against exploratory behavior in T1D mice. Accumulating evidence indicates the central role of AKK bacteria and its therapeutic potential in neuropsychiatric disorders [47]. Zhu et al. reported that metformin treatment improved cognitive impairment in aged mice by enriching the abundance of AKK bacteria and inhibiting the pro-inflammatory cytokine IL-6 [48]. AKK bacteria can also maintain SCFAs-mediated microglial homeostasis and prevent cognitive decline in sleep-deprived mice [49]. Ou et al. found that AKK bacteria effectively relieve disorders in glucolipid metabolism and intestine barrier function, delay amyloid pathology and then improve cognitive deficits in an AD mouse model [50]. Additionally, the protective effect of AKK bacteria on diabetic cognitive decline was also reported in T2D mice via remodeling host metabolism and mitigating neuroinflammation by Du et al. [51]. Herein we elucidated a novel mechanism on the important role of AKK bacteria in the improvement of neuroinflammation and exploratory behavior in T1D mice: AKK bacteria consumed harmful microbial metabolite VB, increased systemic carnitine level, and inhibited neuroinflammation caused by lipid droplet accumulation in microglia. Therefore, the assessment of the levels of AKK bacteria and VB may provide a way to monitor the effectiveness of ADF for improving exploratory behavior in diabetes.

Fasting-driven remodeling of the structure and composition of the gut microbiota has been verified by many studies, but its dynamic changes during fasting represent a complex process [52–54]. Due to the significant reduction in exogenous nutrient intake during fasting, the gut bacteria that depend on host-derived substrates could proliferate and suppress those that rely on dietary substrates [55]. This shift in microbial dynamics may affect the adaptation of the gut microbiota and intestinal cells to the altered nutrient environment induced by fasting. Herein our study revealed that FMT can transfer the beneficial effects of IF, but the non-bacterial components in the fecal suspension also warrant attention. Moreover, the bidirectional regulation between the gut microbiota and host metabolism during IF and FMT is highly complex but cannot be overlooked, which requires further in-depth investigations in the future.

In conclusion, we reported that ADF alleviated neuroinflammation and increased exploratory behavior in T1D mice by enriching AKK bacteria. The beneficial effect of AKK bacteria might be mediated by depleting microbial metabolite VB, increasing systemic carnitine level, reducing microglial lipid droplets and then inhibiting neuroinflammation. Our study uncovered a novel gut-liver-brain metabolic axis mechanism on the protective role of ADF in T1D-induced exploratory behavioral disorders. However, the present study still has some limitations that need to be further explored: (1) The detailed mechanisms underlying AKK bacteria metabolize VB in vivo and whether other microbes or metabolites are also involved in mediating the beneficial effects of IF on neuroinflammation and exploratory behavior can be elucidated in the future; (2) Additional behavioral assessments beyond the OFT would help to further confirm the presence of anxiety-like behavior; (3) Gene-level changes could be validated at the protein level to reinforce the reliability and significance of the findings; (4) It could be interesting to explore the impact of other IF types beyond ADF on neuroinflammation and exploratory behavior in diabetes; (5) The effects of ADF on intestinal metabolism and its potential beneficial outcomes merit further investigations; (6) The safety evaluation of ADF must be carried out prior to its clinical translational application in the prevention and management of exploratory behavioral disorders in T1D patients.

Materials and methods

Animals

In this study, 6-week-old male C57BL/6 mice weighing 20.0 ± 2.0 g were purchased from the Beijing Vital River Laboratory Animal Technology Co., Ltd. and housed in the specific-pathogen-free condition (room temperature = 22 ± 2 °C; humidity = 45 ± 3%; 12-h alternating light cycle) at the Laboratory Animal Center of Wenzhou Medical University. Prior to experiments, mice were acclimated for one week. Mice had free access to standard chow and water, which were pretreated by irradiation and steam autoclave sterilizations, respectively. All animal experiments were conducted according to the Guide for the Care and Use of Laboratory Animals and approved by the Institutional Animal Care and Use Committee of Wenzhou Medical University (ID: xmsq2023-1395).

Streptozotocin-induced diabetic mouse model

After a 12-h fasting, mice were weighed and subjected to an intraperitoneal injection of streptozotocin solution prepared in citrate buffer (0.1 M, pH = 4.5) at a dose of 50 mg/kg body weight for 5 days. The normal control (CON) mice were injected with the same volume of citrate buffer. Afterward, blood glucose level was measured from tail venous after a 3-day streptozotocin injection by using a handheld glucometer (ACCUCHEK Active, Mannheim, Germany). In this study, mice with blood glucose level above 11.1 mmol/L were defined as type 1 diabetic (T1D) mice.

Alternate day fasting (ADF)

Mice were randomly divided into four groups ($n = 12$ per group): (1) CON mice; (2) T1D mice; (3) CON mice with ADF (CON-IF); (4) T1D mice with ADF (T1D-IF). Mice in CON and T1D groups had free access to standard chow, while CON-IF and T1D-IF mice were subjected to an ADF procedure, namely 24 h of fasting followed by 24 h of ad libitum feeding. All mice had free access to water throughout the experiment.

Fecal microbiota transplantation (FMT)

Prior to FMT, the recipient T1D mice were given an antibiotic cocktail, including 0.5 g/L of vancomycin, 1 g/L of metronidazole, 0.2 g/L of ciprofloxacin, and 0.01 g/L of amphotericin B, to deplete their endogenous gut bacteria for one week. Fresh fecal pellets were collected from T1D mice and ADF-treated T1D mice, respectively. To prepare bacterial suspension, the fecal pellets were dissolved in sterile phosphate buffer saline (PBS, 1:7.5, w/v), vortexed for 1 min and centrifuged at 1,000 g for 5 min to remove large particles. Then, the recipient T1D mice were randomly assigned into two groups, and immediately gavaged with 150 μL of the bacterial supernatant from either T1D mice or ADF-treated T1D mice. In this study, FMT was carried out once a day for the first week and every three days for 9 weeks.

Treatment with δ-valerobetaine (VB) or carnitine (CAR)

For VB treatment, CON mice were injected intraperitoneally with either 100 μL of saline vehicle or 100 μL of 5 mM VB (5 mg/kg) once a day for 3 weeks. For CAR treatment, T1D mice were injected intraperitoneally with either 100 μL of saline vehicle or 100 μL of 50 mM VB (50 mg/kg) once a day for 10 weeks.

Supplementation with *Akkermansia muciniphila*

In this study, *A. muciniphila* (ATCC BAA-835) was purchased from the Guangdong Microbial Culture Collection Center (Guangzhou. China) and grown in brain heart infusion (BHI) medium (30 g/L, BD, Sparks, MD) containing 2 g/L of gastrointestinal mucin (Yuanye Biotech, Shanghai, China) and 0.5 g/L of L-cysteine (Sangon Biotech, Shanghai, China) in an anaerobic chamber (10% H_2, 10% CO_2 and 80% N_2) at 37 °C for 48 h. Subsequently, *A. muciniphila* was harvested by centrifuging at 10,000 g for 5 min at 4 °C and suspended in sterile phosphate-buffered saline (PBS, pH = 7.4) containing 10% glycerol, and stored at −80 °C until use. The bacteria were incubated in a BHI medium for 48 h to determine the colony-forming units per milliliter (CFU/mL) under anaerobic conditions. The bacterial concentration was measured by the optical density (OD) at 600 nm and determined to be 5.0×10^8 CFU/mL for an OD value of 1.0. According to the OD value, *A. muciniphila* bacterial suspension was diluted with sterile PBS to a final concentration of 8.0×10^8 CFU per 0.2 mL. Then, T1D mice were orally administered with either 0.2 mL of sterile PBS or bacterial suspension every other day for 8 weeks.

The quantification of *A. muciniphila* by RT-qPCR analysis

Total DNA of fecal samples was extracted by the TIANamp stool DNA kit (DP328-02, TianGen, China) according to the manufacturer's protocol. The concentration of total DNA was measured via a NanoDrop spectrometer (Thermo Fisher Scientific, Beverly, MA). The quantitative detection was performed by the SYBR Premix Ex Taq II kit (Takara, Dalian, China) on LightCycler 480 (Roche, Switzerland). The relative expression level was calculated using the ΔΔCT method and normalized to universal 16S. The specific primer sequences were synthesized by the Tsingke Biotechnology (Beijing, China) as listed in Table S1.

Open field test (OFT)

The OFT was performed to evaluate exploratory behavior of mice in an open-field apparatus (40 × 40 × 40 cm) and the chamber was divided into 16 small squares (10 × 10 cm). Mice were placed in the apparatus center and allowed to a 5-min free exploration. The center area was defined as the region located 10 cm from the wall. The motion trail was recorded via an overhead video system (DigBehav, Jiliang Co. Ltd., Shanghai, China), and the percentages of distance and time in center area as well as the immobile time in edge and center areas were calculated as indicators of exploratory behavior.

Sample collection

Prior to the OFT, fecal samples were harvested into 1.5 mL sterile EP tubes and stored at −80 °C. After the OFT, mice were anaesthetized with isoflurane and sacrificed by rapid decapitation. To obtain serum sample, the whole blood was collected and centrifuged at 1,500 g at 4 °C for 15 min. Since the prefrontal cortex (PFC) is a

major brain region involved in the regulation of exploratory behavior [35], this study focused on this area. Therefore, the PFC and liver tissues were rapidly separated and collected into cryogenic tubes, frozen in liquid nitrogen and kept at −80 °C until use.

Untargeted LC–MS-based metabolomics analysis

Untargeted LC–MS-based metabolomics analysis was carried out according to our previously published method [10]. Frozen brain tissue (10 mg) was weighed into an Eppendorf tube, and 400 μL of methanol (MeOH) and chloroform ($CHCl_3$) were added at a 1:1 (v:v) ratio. The tissue sample was homogenized with a handheld electric homogenizer (FLUKO, Shanghai, China). Serum (20 μL) was transferred into an Eppendorf tube, and 200 μL of MeOH and $CHCl_3$ were added at a 1:1 (v:v) ratio. The mixture was vortexed for 15 s, stood on ice for 15 min, and then centrifuged at 10,000 g for 15 min at 4 °C. Afterward, the supernatant (polar layer) and the lower phase (nonpolar layer) were transferred to new Eppendorf tubes, respectively, dried with a N_2 stream, and stored at −80 °C until analysis. For LC–MS analysis, the dried polar extracts were redissolved in 80 μL of acetonitrile (ACN) and water (v:v = 1:1), while the dried nonpolar extracts were reconstituted in 100 μL of $CHCl_3$ and MeOH (v:v = 1:1). The solution was centrifuged at 15,000 g for 15 min at 4 °C, and the supernatant was transferred to a new Eppendorf tube for analysis.

Metabolomics analysis was performed using a SHIMADZU CBM-30A Lite LC system (Shimadzu, Kyoto, Japan) equipped with an API 6600 Q-TRAP (AB SCIEX, Foster City, CA, USA) under both ESI + and ESI- modes at a mass range of 80–1200 m/z. In this study, we used Waters Acquity amide HILIC column (2.1 × 100 mm, 1.7 μm) and Phenomenex Kinetex C18 column (2.1 × 100 mm, 2.6 μm) to separate polar and lipid metabolites, respectively. The mobile phase for polar compounds consisted of 5 mM ammonium acetate and 0.1% formic acid in water (solvent A) and acetonitrile (solvent B). The gradient elution was set as follows: 0–0.5 min, 98% B; 0.5–13 min, 98–40% B; 13–13.1 min, 40–98% B; 13.1–18 min, 98% B. The mobile phase for lipid compounds consisted of water, MeOH and ACN (v:v:v = 3:1:1) containing 5 mM ammonium acetate (solvent A) and isopropanol (IPA) (solvent B). The gradient elution was used as follows: 0–0.5 min, 25% B; 0.5–1.5 min, 25–40% B; 1.5–3 min, 40–60% B; 3–13 min, 60–98% B; 13–13.1 min, 98–25% B; 13.1–18 min, 25% B. The column temperature was maintained at 40 °C, with an injection volume of 2 μL, a flow rate of 0.3 mL/min and a collision energy of 40 V.

The LC–MS raw data were converted to mzXML format and preprocessed for peak alignment and peak picking using the XCMS software (XCMS plus, CA, USA). The main parameters were used as follows: Bw = 0.1, peak width = 50, Minfrac = 80%, Mzwid = 0.1. Then, three-dimensional raw datasets consisted of *m*/*z* value, retention time, and peak intensity were exported into Microsoft Excel 2020 (Microsoft Corp., Redmond, WA). In this study, peaks with the intensity above 5000 and the coefficient of variation (CV) below 30% were included from further analysis. Metabolites were identified using the MetDNA2 (http://metdna.zhulab.cn/) and One-MAP (http://www.5omics.com/) based on accurate *m*/*z* value and MS/MS fragments. In addition, lipid compounds were identified according to *m*/*z* value and MS/MS fragments in the LipidView software (v1.2, AB Sciex, MA, USA). Lastly, metabolites and lipids were further verified via HMDB 5.0 [56].

Targeted LC–MS analysis

To detect the carnitine and delta-valerobetaine (VB) levels in samples, a MeOH/$CHCl_3$ method was performed according to our previous method [10], and the polar layer was dried with a N_2 stream and stored at −80 °C until usage. The LC–MS analysis was conducted by using a SHIMADZU CBM-30A Lite LC system (Shimadzu, Kyoto, Japan) equipped with an API 6500 Q-TRAP (AB SCIEX, Foster City, CA, USA) under ESI + mode. A Waters Acquity amide HILIC column (2.1 × 100 mm, 1.7 μm) was utilized in this study. The carnitine level was detected in precursor ion scan of *m*/*z* 162.00 and neutral loss of 58.00, and the declustering potential (DP) and collision energy (CE) were set at 20 V and 58 V, respectively. For detecting the VB level, the precursor ion scan of *m*/*z* 160.00 and neutral loss of 101.10 were used, and the DP and CE values were set at 130 V and 22 V, respectively. The linear range of the standard curve was determined to be 1 to 1000 ng/mL with $R^2 > 0.99$.

16S rRNA sequencing analysis

Total microbial DNA in fecal samples was extracted by the TIANamp stool DNA kit following the manufacturer's protocol (TianGen, China). The concentration of total DNA was measured via the agarose gel electrophoresis (AGE, 1%). The V3-V4 region of the 16S rRNA were amplified using the universal primers: 515 F (5'-GTG CCA GCM GCC GCG GTA A-3'); 806R (5'-GGA CTA CHV GGG TWT CTA AT-3'). Afterward, the PCR product was purified according to the manufacturer's protocol of QIAquick gel extraction kit (Qiagen, Germany), and sequenced using an Illumina HiSeq2500 PE250 sequencer (San Diego, USA).

The raw tags were filtered by merging paired-end reads using FLASH software (v1.2.7) and subsequently processed into clean tags through QIIME2 analysis [57]. The

UCHIME algorithm (v7.0.1001) was utilized to generate the effective tags, which were further clustered into operational taxonomic units (OTUs) at a similarity cutoff of 97% with the UPARSE pipeline (v7.0.1001) [58]. The OTUs were annotated on the basis of taxonomic information from the SILVA database using the Mothur method, with a confidence threshold of 80%. Additionally, alpha-and beta-diversity of the gut microbiota were analyzed via the QIIME2 software and R software (v3.5.3).

Cell experiments

BV2 microglia and mouse hepatocytes (AML12) were obtained from the Cell Center of the Institute of Basic Medical Sciences at Chinese Academy of Medical Sciences. The cells were cultured with DMEM medium supplemented with 10% fetal bovine serum and 1% penicillin/streptomycin (C11995500BT, Gibco, Thermo Fisher Scientific, Wilmington, USA) in a humidified 5% CO_2 incubator (Thermo Fisher Scientific) at 37 °C. For cell counting kit-8 (CCK8) assay, the BV2 cells were inoculated in 96-well plates and treated with glucose at the doses of 35, 45, 55 and 65 mM for 12 h to examine the effect of high glucose (HGlu) on the BV2 cell viability. The cells were then incubated with 90 μL of fresh DMEM medium and 10 μL of CCK8 reagent (GK10001, GlpBio, Shanghai, China) at 37 °C in the dark for 1 h. Finally, the cell viability was measured at 450 nm with a Microplate Reader (Thermo Fisher Scientific, Wilmington, USA). In this study, 35 mM glucose was selected as an HGlu condition in vitro. To evaluate the impact of carnitine (CAR) on HGlu-treated BV2 cells, the cells were pretreated with CAR at the doses of 1, 2.5, 5 and 10 μM for 2 h and cultured with 35 mM glucose for 12 h, and then the CCK8 assay was conducted and 5 μM CAR was determined to be the effective dose. Hence, to inspect the effect of CAR on lipid metabolism and inflammatory response in microglia, the BV2 cells were pretreated with 5 μM CAR for 2 h and cultured with 35 mM glucose for 12 h, and then collected for further analysis. To examine the influence of VB on inflammatory response in microglia, the BV2 cells were treated with 100 and 200 μM VB for 12 h and collected for detecting proinflammatory factors. Additionally, the AML12 cells were treated with 100 μM VB for 24 h and then collected for analyzing the effect of VB on carnitine synthesis.

Ex vivo microbial metabolism assay

A. muciniphila was harvested and resuspended in sterile PBS (pH = 7.4) at a concentration of 8.0×10^8 CFU/mL to prepare bacterial suspension. Then, VB was added into either the bacterial suspension or sterile PBS solution, and the concentration of VB was measured by LC–MS at 0, 10 and 20 min.

RT-qPCR analysis

Total RNA of tissue samples was extracted by the Trizol reagent (Invitrogen, USA) based on the manufacturer's protocol. The concentration of total RNA was determined using a NanoDrop spectrometer (Thermo Fisher Scientific, Beverly, MA). Next, cDNA samples were synthesized with the HiScript III RT SuperMix for qPCR (+gDNA wiper) (Vazyme) following the manufacturer's protocol. The quantitative detection was carried out by the SYBR Premix Ex Taq II kit (Takara, Dalian, China) on LightCycler 480 (Roche, Switzerland). The relative expression level was calculated using the ΔΔCT method and normalized to GAPDH. The specific primer sequences were obtained from the Tsingke Biotechnology (Beijing, China) as listed in Table S2.

Histological analysis

The mice ($n = 4$–5 per group) were randomly selected, anesthetized using isoflurane and euthanized following perfusion with normal saline. The prefrontal cortex (PFC) and liver tissues were rapidly harvested and then fixed with 4% paraformaldehyde prepared in PBS buffer (0.1 M, pH = 7.5). The tissue samples were dehydrated by using a graded series of ethanol, embedded in paraffin, and sectioned into 5 μm slices with a slicing machine (Leica, Germany). For immunofluorescence staining, the PFC sections were incubated with Anti-Iba1 antibody (Abcam, ab178846, 1:200) for microglia overnight at 4 °C. The sections were washed using PBS buffer and incubated with secondary antibody goat anti-Rabbit IgG (H + L) (Alexa Fluor 488, Invitrogen, CA, USA) at 37 °C for 1 h. After washing with PBS buffer, the sections were then treated with DAPI (0100–20, Southern Biotech, AL, USA) for 2 min at 22 °C. For immunohistochemistry analysis, the sections were dewaxed using xylene, rehydrated in a series of graded alcohol solutions, and incubated with 4-hydroxynonenal (4-HNE) (Abcam, ab46545, 1:200) for the prefrontal cortex or the primary antibody BBOX (Affinity Biosciences, 1:100) for the liver tissue overnight at 4 °C. Subsequently, the sections were washed with PBS buffer for three times, incubated with goat anti-mouse/rabbit IgG secondary antibodies conjugated with horseradish peroxidase (HRP) for 1 h at 37 °C, and stopped by 3,3'-diaminobenzidine (DAB) chromogen kit (ZLI-9018, ZSGB-BIO, Beijing, China). For Nissl staining, the PFC sections were dewaxed in xylene, rehydrated with a series of graded alcohol solutions, and stained using 0.1% cresyl violet for 10 min. After washing with PBS buffer, the sections were differentiated in 95% ethyl alcohol for 5 min, dehydrated with a series of graded alcohol solutions,

cleared in xylene and then mounted with neutral resin. Lastly, images were acquired by a Nikon ECLIPSE NI microscope (Nikon, Tokyo, Japan) and the positive staining areas were quantified using ImageJ software (v1.47, Bethesda, MD, USA) with the Huang algorithm and the threshold set to 0–155 intensity. Group information was masked during the quantification process.

For microglial lipid droplet staining, the PFC samples were removed from paraformaldehyde, dehydrated with a graded series of 15%–30% sucrose in PBS, and then embedded in a cryomold using an optimum cutting temperature (OCT) compound. The samples were quickly placed in liquid nitrogen for rapid freezing and sectioned into 10 μm slices using a cryostat (Cryostar NX70, Thermo Fisher Scientific, Bremen, Germany). Later, the PFC sections were equilibrated to room temperature, washed with PBS buffer, and incubated overnight at 4 °C with an Anti-Iba1 antibody (Abcam, ab178846, 1:200). After washing in PBS buffer, the sections were incubated with a secondary antibody goat anti-rabbit IgG (H + L) (Alexa Fluor 594, Invitrogen, CA, USA) at 37 °C for 1 h and BODIPY™ 493/503 (Thermo Fisher Scientific, D3922, 1:1000) at 22 °C for 20 min. After washing with PBS buffer, the sections were treated with DAPI (0100–20, Southern Biotech, AL, USA) for 2 min at 22 °C. Finally, images were captured using a confocal laser scanning microscope (C2si, Nikon, Tokyo, Japan) and the positive staining areas were quantified using ImageJ software (v1.47, Bethesda, MD, USA) with the Huang algorithm and the threshold set to 50–255 intensity. Group information was masked during the quantification process.

Data analysis and statistics

All mice were randomly assigned to the experimental procedures including animal grouping, treatment, sample collection and data analysis. Omics data were subjected to log-transformation and Pareto-scaling prior to multivariable analysis. For metabolomics data analysis, principal component analysis (PCA) was used to examine the changes in metabolic patterns among different groups with SIMCA-P + software (v12.0, Umetrics AB, Umea, Sweden). Orthogonal projection to latent structures discriminant analysis (OPLS-DA) was then performed to maximize the metabolic differentiation between two groups and identify key metabolites based on the variable importance in the projection (VIP > 1.0) method via the SIMCA-P + software. The alpha-diversity of the gut microbiota between different groups was analyzed by principal coordinate analysis (PCoA) with Bray–Curtis distance in R software (v2.15.3).

For univariate data analysis, the statistic difference between two groups was evaluated by two-tailed unpaired student's *t* test using SPSS 22.0 software (SPSS, Inc., Chicago, IL, USA). The statistic difference among different groups was analyzed by one-way ANOVA with a post-hoc Dunnett's test for multiple comparisons. In this study, a statistically significant difference was considered when $p < 0.05$. The volcano plot analysis was constructed by plotting $\log_2$ (FC, fold change) versus $-\log_{10}$ (P) in the R software. The metabolite set enrichment analysis was used to achieve the functional classification of metabolites based on the KEGG pathway database using MetaboAnalyst 6.0 [59].

Abbreviations

4-HNE	4-Hydroxynonenal
ADF	Alternate day fasting
AKK	*Akkermansia muciniphila*
BBOX	γ-Butyrobetaine hydroxylase
CAR	Carnitine
CON	Normal control
FAO	Fatty acid oxidation
FMT	Fecal microbiota transplant
IF	Intermittent fasting
OFT	Open field test
PFC	Prefrontal cortex
T1D	Type 1 diabetic
VB	δ-Valerobetaine

Supplementary Information

The online version contains supplementary material available at https://doi.org/10.1186/s40168-025-02196-6.

Supplementary Material 1. **Table S1.** Specific primer pairs for Akkermansia muciniphila analysis. **Table S2.** Specific primer pairs for RT-qPCR analysis. **Figure S1.** Changes in basic physiological data of T1D mice. **Figure S2.** The effect of alternate day fasting on basic physiological data in mice. **Figure S3.** Identification of key gut microbes in T1D mice after alternate day fasting. **Figure S4.** Alternate day fasting reshapes host metabolism in T1D mice. **Figure S5.** Metabolic changes in the prefrontal cortex and serum of T1D mice after alternate day fasting. **Figure S6.** The effect of δ-valerobetaine on carnitine synthesis in AML12 cells. **Figure S7.** Alterations in the gut microbiota in T1D mice after fecal microbiota transplant. **Figure S8.** Fecal microbiota transplant reduces neuroinflammation and neuron injury in the prefrontal cortex (PFC) of T1D mice. **Figure S9.** The effects of high glucose and carnitine on the BV2 cell viability. **Figure S10.** The effect of carnitine on lipid droplets in high glucose-treated BV2 cells. **Figure S11.** The effect of carnitine on inflammatory response in high glucose (HGlu)-treated BV2 cells. **Figure S12.** The effect of carnitine on lipid metabolism in high glucose (HGlu)-treated BV2 cells. **Figure S13.** The effect of δ-valerobetaine (VB) on inflammatory response in BV2 cells.

Acknowledgements

We are grateful for the help from the Scientific Research Center and the Laboratory Animal Center of Wenzhou Medical University.

Authors' contributions

HZ contributed to the experimental design. KYG, MJW and XLY contributed to animal and cell experiments. KYG, MJW, XLY, YJP and QPC contributed to sample collection and metabolomics analysis. KYG, JHM and HJ contributed to experiments related to Akkermansia muciniphila. KYG, YJP, QPC and SHZ contributed to analyses of molecular biology and histological analysis. HZ, KYG, HJ, ZW and WJW contributed to result discussion and interpretation. HZ and KYG contributed to the data analysis and draft writing. SHZ, YJP and QPC contributed to the major revision of manuscript. All authors have read, revised and approved the final manuscript.

Funding
This study was supported by the Zhejiang Provincial Natural Science Foundation of China (No.: LY23H090008) and National Natural Science Foundation of China (No.: 22074106).

Data availability
Metabolomics data have been deposited into Figshare and can be freely downloaded at https://doi.org/10.6084/m9.figshare.26788627.v1. The microbiota raw sequencing data have been uploaded to the NCBI SRA database with the accession number PRJNA1180212. Other data and materials are present in the main text and supplementary materials.

Declarations

Ethics approval and consent to participate
All animal experiments were conducted according to the Guide for the Care and Use of Laboratory Animals and approved by the Institutional Animal Care and Use Committee of Wenzhou Medical University (ID: xmsq2023-1395).

Consent for publication
Not applicable.

Competing interests
The authors declare no competing interests.

Author details
[1]State Key Laboratory of Macromolecular Drugs and Large-Scale Preparation, School of Pharmaceutical Sciences, Wenzhou Medical University, Wenzhou 325035, China. [2]Institute of Life Sciences, College of Life and Environmental Science, Wenzhou University, Wenzhou 325035, China. [3]Department of Neurology, The First Affiliated Hospital of Wenzhou Medical University, Wenzhou 325000, China. [4]Department of Endocrinology and Metabolism, The First Affiliated Hospital of Wenzhou Medical University, Wenzhou 325000, China.

Received: 11 October 2024 Accepted: 11 July 2025
Published online: 09 October 2025

References

1. Gregory GA, Robinson TI, Linklater SE, Wang F, Colagiuri S, de Beaufort C, et al. Global incidence, prevalence, and mortality of type 1 diabetes in 2021 with projection to 2040: a modelling study. Lancet Diabetes Endocrinol. 2022;10(10):741–60.
2. Amidei CB, Fayosse A, Dumurgier J, Machado-Fragua MD, Tabak AG, van Sloten T, et al. Association between age at diabetes onset and subsequent risk of dementia. JAMA. 2021;325(16):1640–9.
3. Dove A, Wang J, Huang H, Dunk MM, Sakakibara S, Guitart-Masip M, et al. Diabetes, prediabetes, and brain aging: the role of healthy lifestyle. Diabetes Care. 2024;47(10):1794–802.
4. Dutta BJ, Singh S, Seksaria S, Gupta GD, Singh A. Inside the diabetic brain: Insulin resistance and molecular mechanism associated with cognitive impairment and its possible therapeutic strategies. Pharmacol Res. 2022;182: 106358.
5. Bhatti JS, Sehrawat A, Mishra J, Sidhu IS, Navik U, Khullar N, et al. Oxidative stress in the pathophysiology of type 2 diabetes and related complications: Current therapeutics strategies and future perspectives. Free Radic Biol Med. 2022;184:114–34.
6. Carvalho C, Cardoso S. Diabetes-Alzheimer's disease link: Targeting mitochondrial dysfunction and redox imbalance. Antioxid Redox Signal. 2021;34(8):631–49.
7. Cheng LZ, Li W, Chen YX, Lin YJ, Miao Y. Autophagy and diabetic encephalopathy: mechanistic insights and potential therapeutic implications. Aging Dis. 2022;13(2):447.
8. Sun Y, Ma C, Sun H, Wang H, Peng W, Zhou Z, et al. Metabolism: a novel shared link between diabetes mellitus and Alzheimer's disease. J Diabetes Res. 2020;2020(1):4981814.
9. Su WJ, Li JM, Zhang T, Cao ZY, Hu T, Zhong SY, et al. Microglial NLRP3 inflammasome activation mediates diabetes-induced depression-like behavior via triggering neuroinflammation. Prog Neuropsychopharmacol Biol Psychiatry. 2023;126: 110796.
10. Xiong F, Gong K, Xu H, Tu Y, Lu J, Zhou Y, et al. Optimized integration of metabolomics and lipidomics reveals brain region-specific changes of oxidative stress and neuroinflammation in type 1 diabetic mice with cognitive decline. J Adv Res. 2023;43:233–45.
11. Tilg H, Zmora N, Adolph TE, Elinav E. The intestinal microbiota fuelling metabolic inflammation. Nat Rev Immun. 2020;20(1):40–54.
12. Chen C, Liao J, Xia Y, Liu X, Jones R, Haran J, et al. Gut microbiota regulate Alzheimer's disease pathologies and cognitive disorders via PUFA-associated neuroinflammation. Gut. 2022;71(11):2233–52.
13. Xu Q, Sun L, Chen Q, Jiao C, Wang Y, Li H, et al. Gut microbiota dysbiosis contributes to depression-like behaviors via hippocampal NLRP3-mediated neuroinflammation in a postpartum depression mouse model. Brain Behav Immun. 2024;119:220–35.
14. Ma J, Li M, Bao Y, Huang W, He X, Hong Y, et al. Gut microbiota-brain bile acid axis orchestrates aging-related neuroinflammation and behavior impairment in mice. Pharmacol Res. 2024;208: 107361.
15. Zhao Q, Chen J, Wu M, Yin X, Jiang Q, Gao H, et al. Microbiota from healthy mice alleviates cognitive decline via reshaping the gut-brain metabolic axis in diabetic mice. Chem Biol Interact. 2023;382: 110638.
16. Ye XX, Jiang QY, Wu MJ, Ye QH, Zheng H. Transplant of fecal microbiota from healthy young mice relieves cognitive defects in late-stage diabetic mice by reducing metabolic disorders and neuroinflammation. Acta Pharmacol Sin. 2024;45(12):2513–26.
17. Sampson TR, Debelius JW, Thron T, Janssen S, Shastri GG, Ilhan ZE, et al. Gut microbiota regulate motor deficits and neuroinflammation in a model of Parkinson's disease. Cell. 2016;167(6):1469–80.
18. Sun J, Zhang Y, Kong Y, Ye T, Yu Q, Satyanarayanan SK, et al. Microbiota-derived metabolite Indoles induced aryl hydrocarbon receptor activation and inhibited neuroinflammation in APP/PS1 mice. Brain Behav Immun. 2022;106:76–88.
19. Qian X, Hai W, Chen S, Zhang M, Jiang X, Tang H. Multi-omics data reveals aberrant gut microbiota-host glycerophospholipid metabolism in association with neuroinflammation in APP/PS1 mice. Gut Microbes. 2023;15(2):2282790.
20. Wu L, Han Y, Zheng Z, Zhu S, Chen J, Yao Y, et al. Obeticholic acid inhibits anxiety via alleviating gut microbiota-mediated microglia accumulation in the brain of high-fat high-sugar diet mice. Nutrients. 2021;13(3):940.
21. Cross C, Davies M, Bateman E, Crame E, Joyce P, Wignall A, et al. Fibre-rich diet attenuates chemotherapy-related neuroinflammation in mice. Brain Behav Immun. 2024;115:13–25.
22. Sun P, Wang M, Li Z, Wei J, Liu F, Zheng W, et al. *Eucommiae cortex* polysaccharides mitigate obesogenic diet-induced cognitive and social dysfunction via modulation of gut microbiota and tryptophan metabolism. Theranostics. 2022;12(8):3637.
23. Liu D, Zhu Y, Hou Z, Wang H, Li Q. Polysaccharides from *Astragalus membranaceus* Bunge alleviate LPS-induced neuroinflammation in mice by modulating microbe-metabolite-brain axis and MAPK/NF-κB signaling pathway. Int J Biol Macromol. 2025;304: 140885.
24. Sun J, Xu J, Yang B, Chen K, Kong Y, Fang N, et al. Effect of *Clostridium butyricum* against microglia-mediated neuroinflammation in Alzheimer's disease via regulating gut microbiota and metabolites butyrate. Mol Nutr Food Res. 2020;64(2):1900636.
25. Kong Q, Chen Q, Mao X, Wang G, Zhao J, Zhang H, et al. *Bifidobacterium longum* CCFM1077 ameliorated neurotransmitter disorder and neuroinflammation closely linked to regulation in the kynurenine pathway of autistic-like rats. Nutrients. 2022;14(8):1615.
26. Qian X, Li Q, Zhu H, Chen Y, Lin G, Zhang H, et al. Bifidobacteria with indole-3-lactic acid-producing capacity exhibit psychobiotic potential via reducing neuroinflammation. Cell Rep Med. 2024;5(11): 101798.
27. Chen L, Tian FY, Hu XH, Wu JW, Xu WD, Huang Q. Intermittent fasting in type 2 diabetes: from fundamental science to clinical applications. Eur Rev Med Pharmacol Sci. 2023;27(1):333–51.
28. Liu J, Shao N, Qiu H, Zhao J, Chen C, Wan J, et al. Intestinal microbiota: A bridge between intermittent fasting and tumors. Biomed Pharmacother. 2023;167: 115484.
29. Shi H, Zhang B, Abo-Hamzy T, Nelson JW, Ambati CSR, Petrosino JF, et al. Restructuring the gut microbiota by intermittent fasting lowers blood pressure. Circ Res. 2021;128(9):1240–54.

30. Cignarella F, Cantoni C, Ghezzi L, Salter A, Dorsett Y, Chen L, et al. Intermittent fasting confers protection in CNS autoimmunity by altering the gut microbiota. Cell Metab. 2018;27(6):1222–35.
31. Li G, Xie C, Lu S, Nichols RG, Tian Y, Li L, et al. Intermittent fasting promotes white adipose browning and decreases obesity by shaping the gut microbiota. Cell Metab. 2017;26(4):672–85.
32. Gudden J, Arias Vasquez A, Bloemendaal M. The effects of intermittent fasting on brain and cognitive function. Nutrients. 2021;13(9):3166.
33. Pan RY, Zhang J, Wang J, Wang Y, Li Z, Liao Y, et al. Intermittent fasting protects against Alzheimer's disease in mice by altering metabolism through remodeling of the gut microbiota. Nat Aging. 2022;2(11):1024–39.
34. Guo M, Wang X, Li Y, Luo A, Zhao Y, Luo X, et al. Intermittent fasting on neurologic diseases: potential role of gut microbiota. Nutrients. 2023;15(23):4915.
35. Dong W, Chen H, Sit T, Han Y, Song F, Vyssotski AL, et al. Characterization of exploratory patterns and hippocampal-prefrontal network oscillations during the emergence of free exploration. Sci Bull. 2021;66(21):2238–50.
36. Liu KH, Owens JA, Saeedi B, Cohen CE, Bellissimo MP, Naudin C, et al. Microbial metabolite delta-valerobetaine is a diet-dependent obesogen. Nat Metab. 2021;3(12):1694–705.
37. Zhao M, Zhao L, Xiong X, He Y, Huang W, Liu Z, et al. TMAVA, a metabolite of intestinal microbes, is increased in plasma from patients with liver steatosis, inhibits γ-butyrobetaine hydroxylase, and exacerbates fatty liver in mice. Gastroenterology. 2020;158(8):2266–81.
38. Longo N, Frigeni M, Pasquali M. Carnitine transport and fatty acid oxidation. BBA Mol Cell Res. 2016;1863(10):2422–35.
39. Liu Z, Dai X, Zhang H, Shi R, Hui Y, Jin X, et al. Gut microbiota mediates intermittent-fasting alleviation of diabetes-induced cognitive impairment. Nat Commun. 2020;11(1):855.
40. Marschallinger J, Iram T, Zardeneta M, Lee SE, Lehallier B, Haney MS, et al. Lipid-droplet-accumulating microglia represent a dysfunctional and proinflammatory state in the aging brain. Nat Neurosci. 2020;23(2):194–208.
41. Wang W, Pan D, Liu Q, Chen X, Wang S. L-carnitine in the treatment of psychiatric and neurological manifestations: a systematic review. Nutrients. 2024;16(8):1232.
42. Haikonen R, Kärkkäinen O, Koistinen V, Hanhineva K. Diet- and microbiota-related metabolite, 5-aminovaleric acid betaine (5-AVAB), in health and disease. Trends Endocrinol Metab. 2022;33(7):463–80.
43. Zhao M, Wei H, Li C, Zhan R, Liu C, Gao J, et al. Gut microbiota production of trimethyl-5-aminovaleric acid reduces fatty acid oxidation and accelerates cardiac hypertrophy. Nat Commun. 2022;13(1):1757.
44. Haberbosch L, Kierszniowska S, Willmitzer L, Mai K, Spranger J, Maurer L. 5-Aminovaleric acid betaine predicts impaired glucose metabolism and diabetes. Nutr Diabetes. 2023;13(1):17.
45. Kim J, Naudin C, Liu K, Parcha K, Dawson P, Jones R, et al. Gut microbial metabolite delta-valerobetaine (VB) influences energy metabolism by altering fat utilization and satiety-related hormones in mice. Physiology. 2023;38:5727905.
46. Mossad O, Nent E, Woltemate S, Folschweiller S, Buescher JM, Schnepf D, et al. Microbiota-dependent increase in δ-valerobetaine alters neuronal function and is responsible for age-related cognitive decline. Nat Aging. 2021;1(12):1127–36.
47. Xu R, Zhang Y, Chen S, Zeng Y, Fu X, Chen T, et al. The role of the probiotic *Akkermansia muciniphila* in brain functions: insights underpinning therapeutic potential. Crit Rev Microbiol. 2023;49(2):151–76.
48. Zhu X, Shen J, Feng S, Huang C, Wang H, Huo F, et al. *Akkermansia muciniphila,* which is enriched in the gut microbiota by metformin, improves cognitive function in aged mice by reducing the proinflammatory cytokine interleukin-6. Microbiome. 2023;11(1):120.
49. Li N, Tan S, Wang Y, Deng J, Wang N, Zhu S, et al. *Akkermansia muciniphila* supplementation prevents cognitive impairment in sleep-deprived mice by modulating microglial engulfment of synapses. Gut Microbes. 2023;15(2):2252764.
50. Ou Z, Deng L, Lu Z, Wu F, Liu W, Huang D, et al. Protective effects of *Akkermansia muciniphila* on cognitive deficits and amyloid pathology in a mouse model of Alzheimer's disease. Nutr Diabetes. 2020;10(1):12.
51. Du Y, An Y, Song Y, Li N, Zheng J, Lu Y. Live and pasteurized *Akkermansia muciniphila* ameliorates diabetic cognitive impairment by modulating gut microbiota and metabolites in db/db mice. Exp Neurol. 2024;378:114823.
52. Li L, Su Y, Li F, Wang Y, Ma Z, Li Z, et al. The effects of daily fasting hours on shaping gut microbiota in mice. BMC Microbiol. 2020;20(1):65.
53. Pérez-Gerdel T, Camargo M, Alvarado M, Ramírez JD. Impact of intermittent fasting on the gut microbiota: a systematic review. Adv Biol. 2023;7(8): e2200337.
54. Paukkonen I, Törrönen EN, Lok J, Schwab U, El-Nezami H. The impact of intermittent fasting on gut microbiota: a systematic review of human studies. Front Nutr. 2024;11:1342787
55. Ducarmon QR, Grundler F, Le Maho Y, Wilhelmi de Toledo F, Zeller G, Habold C, et al. Remodelling of the intestinal ecosystem during caloric restriction and fasting. Trends Microbiol. 2023;31(8):832–44.
56. Wishart DS, Guo A, Oler E, Wang F, Anjum A, Peters H, et al. HMDB 5.0: the human metabolome database for 2022. Nucleic Acids Res. 2022;50:D622-D631.
57. Bolyen E, Rideout JR, Dillon MR, Bokulich NA, Abnet CC, Al-Ghalith GA, et al. Reproducible, interactive, scalable and extensible microbiome data science using QIIME 2. Nat Biotechnol. 2019;37(8):852–7.
58. Edgar RC. UPARSE: highly accurate OTU sequences from microbial amplicon reads. Nat Methods. 2013;10(10):996–8.
59. Pang Z, Lu Y, Zhou G, Hui F, Xu L, Viau C, et al. MetaboAnalyst 6.0: towards a unified platform for metabolomics data processing, analysis and interpretation. Nucleic Acids Res. 2024;52:W398-W406.

Publisher's Note